

**Experimental and theoretical investigation on the extractive mass transfer of Eu<sup>3+</sup> ions using novel amide ligands in 1-hexyl-3-methylimidazolium bis(trifluoromethylsulfonyl)imide**

**Ayan Ghosh<sup>a,#</sup>, Amit Pandey<sup>b,#</sup>, Arijit Sengupta<sup>\*,c,d</sup>, Velavan Kathirvelu<sup>b</sup>, Sarvesh S. Harmalkar<sup>e</sup>, Sunder N. Dhuri<sup>e</sup>, Keisham S. Singh<sup>f</sup>, Tapan K. Ghanty<sup>\*,d,g</sup>**

<sup>a</sup>Laser and Plasma Technology Division, Beam Technology Development Group, Bhabha Atomic Research Centre, Trombay, Mumbai-400085, India;

<sup>b</sup>Department of Applied Sciences, National Institute of Technology Goa, Ponda, Goa 403 401, India;

<sup>c</sup>Radiochemistry Division, Bhabha Atomic Research Centre, Trombay, Mumbai-400085, India;

<sup>d</sup>HomiBhabha National Institute, Anushaktinagar, Mumbai-400094, India;

<sup>e</sup>School of Chemical Sciences, Goa University, Goa 403 206;

<sup>f</sup>Bioorganic Chemistry Laboratory, CSIR-National Institute of Oceanography, Dona Paula, Goa 403 004, India;

<sup>g</sup>Bio-Science Group, Bhabha Atomic Research Centre, Trombay, Mumbai-400085, India

corresponding author: arijita@barc.gov.in; arijitbarc@gmail.com and tapang@barc.gov.in;

# these authors contributed equally

**Abstract**

Novel amide ligands in the ionic liquid (1-hexyl-3-methylimidazolium bis(trifluoromethylsulfonyl)imide) were utilized for the liquid-liquid biphasic mass transfer of Eu<sup>3+</sup> ions from aqueous acidic waste solution. The cation exchange mechanism was found to be operative with the formation of [Eu(NO<sub>3</sub>)<sub>2</sub>L<sub>3</sub>]<sup>+</sup> species (L = 4-chloro-N-(1-methyl-1H-pyrazol-3-yl)picolinamide). However, the presence of an inner-sphere water molecule was revealed by DFT calculation. The viscosity induced slower kinetics was evidenced during mass transfer, which was improved by increasing temperature. The process was exothermic in nature. The improvement in the kinetics of extractive mass transfer at higher temperatures is evinced by a reduction in the distribution ratio value. The spontaneity of the reaction was evidenced through negative Gibbs energy value, whereas the process enhances the entropy of the system, probably by releasing water molecules at least partially during complexation. The structures of bare ligands and complexes have been optimized by density functional theory (DFT) calculations. A high value of complexation energy, solvation energy and associated enthalpy and free energy change reveal the efficacy in binding Eu with O and N donor atoms. In addition, the natural population analysis (NPA), atoms-in-molecules (AIM) analysis, and energy decomposition analysis (EDA) have been employed to explore the nature of bonding existing in Eu–O and Eu–N bonds.

**Keywords:** Ionic liquid; Cation exchange; Spontaneous; Exothermic; Density Functional Theory

## Introduction

Nuclear energy is considered a renewable and green energy source with tremendous potential to cater to global energy needs. However, the success story lies in safely managing highly toxic nuclear waste, its storage, disposal, and associated public acceptance<sup>1</sup>. Trivalent lanthanides and minor actinides are the typical elements generated during nuclear fission in the reactor. Therefore, the development of separation strategies for trivalent f-block elements is highly desirable. Diamide, phosphine oxides, glycolamides, and their derivatives are well exploited to serve the purpose<sup>2</sup>. In the present investigation, novel amide ligands have been synthesized and applied for extractive mass transfer of trivalent f-block element,  $\text{Eu}^{3+}$ . The separation processes are mostly based on liquid-liquid biphasic extractive mass transfer involving volatile organic compounds (VOCs) as diluents or solid-liquid sorption-based chromatographic separation<sup>3</sup>. The solid phase-based separations are well adopted on a laboratory scale but challenging to be adopted on a commercial/large scale. On the other hand, this technique is good for analytical separation. The first approach can be exploited for large-scale separation in batch and continuous modes of operation<sup>4</sup>. Handling such a large number of VOCs is of environmental concern and accident-prone due to their flash point and thermal/chemical instability.

Ionic liquid gained worldwide acceptance as a potential replacement for VOCs<sup>5</sup>. The lower lattice energy associated with their charge delocalization leads to their existence in liquid form even though ionic in nature. Separation of actinides in different oxidation states using ionic liquids in combination with specific ligands has been found in the literature to improve the efficiency of extraction<sup>6</sup>. To impose specificity, certain functional groups have been covalently anchored into the ionic liquid cations<sup>7</sup>. Diglycolamide and carbamoyl phosphine oxide functionalized ionic liquids have demonstrated a high affinity for trivalent actinides. Whereas phosphate functionalized ionic liquid exhibited higher affinity towards hexavalent uranyl ion<sup>8</sup>. Apart from the 'green' separation, ionic liquids have demonstrated the tunability of extraction characteristics by structural modification either in their cationic or anionic part<sup>9</sup>. The substituent at the C3 position in methyl imidazolium cation-based ionic liquid can be exploited for tuning the solvation mechanism to a cation exchange mechanism of mass transfer. For uranyl ions with the same amide ligand, the extraction mechanism can be a solvation, cation exchange, or anion exchange mechanism by changing the cations of ionic liquid<sup>10</sup>. The speciation and thermodynamic parameters associated with extraction differed in ionic liquid compared to molecular diluents<sup>11</sup>. The viscosity-based tuning in extraction kinetics in ionic liquid has also been demonstrated<sup>12</sup>. Polyionic liquid and ionic liquid-based membranes exhibit non-conventional separation based on pi-pi interaction, unlike the molecular sieving mechanism<sup>13</sup>.

Ionic liquid-based solvent systems exhibited high radiation stability, which is one of the preferred features for processing radioactive materials<sup>14</sup>. The continuous emission of high-energy gamma radiation or alpha and beta particles deposits enormous energy into the solvent system. This can lead to deterioration of separation performance, especially for molecular diluent-based systems. However, the ionic liquids were reported to act as a radiation sink. Hence, the functionality responsible for metal ion complexation remained unmodified, i.e., minimal radiation-induced performance deterioration is observed in ionic liquid-based systems. The formation of resonance-stabilized radicals and radical cations is proposed to be responsible for such high radiolytic stability<sup>15</sup>.

In view of the above facts, some novel amide-based ligands in ionic liquids (1-hexyl-3-methylimidazolium bis(trifluoromethylsulfonyl)imide) have been exploited for  $\text{Eu}^{3+}$  ions extraction in the present study. Furthermore, experimental and computational approaches were employed to understand the mechanism of extraction, speciation, and energy associated with the liquid-liquid biphasic extractive mass transfer.

## **Experimental**

### ***Materials***

All the materials used in the present investigations are of analytical grade unless otherwise mentioned. Deionized (DI) water was used throughout the experiments. Suprapur nitric acid procured from E-Merck, Germany, was used for varying the feed acidity of the aqueous phase. ICP standard Eu in nitric acid with an initial concentration of  $1 \text{ mg mL}^{-1}$  was used as Eu stock. This solution was also purchased from E-Merck, Germany. The ionic liquids, 1-hexyl-3-methylimidazolium bis(trifluoromethylsulfonyl)imide ( $\text{C}_6\text{mimNTF}_2$ ) and 1-hexyl-3-methylimidazolium bromide were procured from TCI Chemical Pvt Ltd., India. The Li salt of bis(trifluoromethylsulfonyl)imide ( $\text{LiNTF}_2$ ) was purchased from Sigma Aldrich. 5-Bromoisophthalic acid, 6-Amino-2,4-lutidine, isopropyl amine, 4-Chloropicolinic acid, and triethylamine were purchased from TCI Chemicals. Dichloromethane and thionylchloride were purchased from SRL Chemicals. The solvents were freshly distilled before use.

### **Instrumentation**

The liquid-liquid biphasic separation experiments were carried out using thermostated water bath purchased from Lab Enterprise, Mumbai, India. This temperature-controlled shaker can be operated between ambient temperature and  $90^\circ\text{C}$  with temperature precision  $\pm 0.1^\circ\text{C}$ . The centrifuge machine used for separating the aqueous and organic phases was procured from Lab Enterprise, Mumbai,

India. Energy Dispersive X-ray Fluorescence Spectroscopy (EDXRF) was used for Eu determination. This spectrometer was procured from Jordan Valley, EX 3600, Israel. The Be window, Rh source, Si-Li detector were employed for X-ray excitation, emission, and signal measurements. The optimized instrumental and experimental parameters were summarized elsewhere<sup>16</sup>. NMR spectra were recorded on a Bruker Advance spectrometer at 400 MHz (<sup>1</sup>H) and 100 MHz (<sup>13</sup>C) with SiMe<sub>4</sub> as internal references. The IR spectrum was recorded on IR Affinity-1, Fourier Transform Infrared Spectrophotometer (Shimadzu). The mass spectrum was collected on LC-MS (Shimadzu) instrument. CHNS analysis of the ligand was carried out in Elementar vario MICRO cube CHNS Analyzer. The crystal structure of 4-Chloro-N-(1-methyl-1H-pyrazol-3-yl)picolinamide (L<sup>4</sup>) was determined using a Bruker D8 Quest Eco X-ray diffractometer. Intensity data were collected at room temperature (RT) using monochromated (MoK $\alpha$ = 0.7107 Å) radiation. The program suite APEX3 (version 2018.1) was used to integrate the frames, perform absorption correction, and determine unit cell. The structure was solved, and subsequent refinement was performed with SHELXL<sup>17</sup>. The non-hydrogen atoms were refined with the anisotropic displacement parameters, while the hydrogen atoms were located at the calculated positions.

### *Synthesis of ligands*

5-bromoisophthalamide ligands (L<sup>1</sup> - L<sup>3</sup>): These ligands were synthesized and characterized as described in the literature<sup>10, 18</sup>. The general procedure for synthesising ligands involves a two-step reaction [Fig. 1]. Initially, thionyl chloride (40 mmol, 2.90 mL) was added to 5-bromoisophthalic acid (2 mmol, 0.490 g), and the suspension was refluxed under a nitrogen atmosphere for 16 h to give a clear solution. Then, the resulting solution was dried under a vacuum to give the acid chloride.

The colourless viscous 5-bromoisophthaloyldichloride (2.0 mmol) liquid was dissolved in dry dichloromethane (10 mL) and cooled to 0°C. A solution of amine (R-NH<sub>2</sub>, 4.0 mmol) and triethylamine (8.0 mmol, 1.12 mL) in dry DCM (5 mL) was added drop by drop. The resulting mixture was stirred at room temperature under a nitrogen atmosphere for 16 h and dried under a vacuum. The residue was dissolved in dichloromethane and washed with an aqueous ammonium chloride solution followed by water. The organic phase was dried in anhydrous Na<sub>2</sub>SO<sub>4</sub> and evaporated to dryness, yielding the corresponding amide (L<sup>1</sup> - L<sup>3</sup>, Fig. 1). Purification was performed by column chromatography on silica gel.

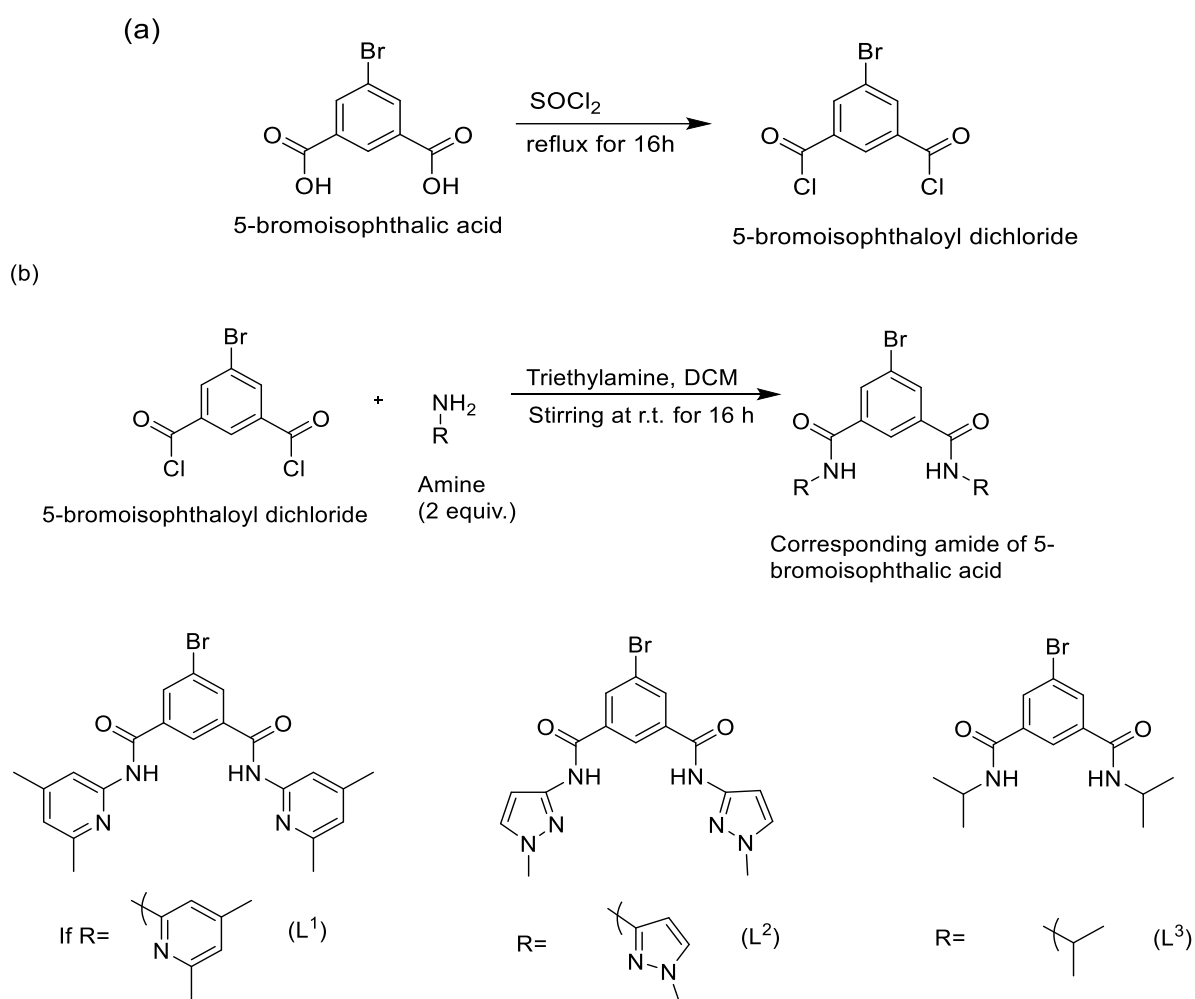


**Fig.1:** Synthetic route for (a) 5-bromoisophthaloyl dichloride and (b) 5-bromoisophthalamide ligands (L<sup>1</sup> – L<sup>3</sup>)

*4-Chloro-N-(1-methyl-1H-pyrazol-3-yl)picolinamide (L<sup>4</sup>):* A suspension of 4-chloropicolinic acid (2 mmol, 0.315 g) and thionyl chloride (20 mmol, 1.45 mL) in a round bottom flask was refluxed under nitrogen atmosphere for 16 h. to give an orange-coloured solution<sup>19</sup>. Excess thionyl chloride was removed in a vacuum to give an orange viscous liquid, 4-chloropicolinoyl chloride. Then, the acid chloride was dissolved in dry dichloromethane (10 mL) and cooled to 0°C. A solution of 3-amino-1-methylpyrazole (2.0 mmol, 0.175 mL) and triethylamine (8.0 mmol, 1.1 mL) in dry dichloromethane (5 mL) was added to the acid chloride solution drop by drop. Then, the mixture was stirred at room temperature under a nitrogen atmosphere for 16 h. The reaction mixture was then dried under a vacuum. The residue was dissolved in dichloromethane and washed with aqueous ammonium chloride solution, followed by water. The organic phase was dried with anhydrous Na<sub>2</sub>SO<sub>4</sub>, and rotary evaporated to dryness, yielding L<sup>4</sup> (**Fig.2**). Purification by silica gel column chromatography using petroleum ether and ethyl acetate (0 to 30%) mixture as eluent afforded 0.354 g (75 %) of L<sup>4</sup>, as white solid (**Fig. 2**). Rf

= 0.65, TLC (eluent: Petroleum ether/ethyl acetate 60:40 v/v). FTIR (KBr,  $\text{cm}^{-1}$ ): 3342 (s, N–H str. amide), 3111 (C–H str. aromatic), 2935 (s, C–H str. alkyl), 1680 (s, C=O str. Amide), 1566 (s, N–H bend amide), 1556–1427 (C=C str. aromatic), 756 (C–Cl str.) [Supplementary Fig. S1].  $^1\text{H NMR}$  (400 MHz,  $\text{CDCl}_3$ )  $\delta$ : 10.254 (s, 1H, NH amide), 8.501–8.488 (d, 1H, pyr CH), 8.262–8.257 (d, 1H, pyr CH), 7.473–7.455 (m, 1H, pyr CH), 7.317–7.311 (d, 1H, pyrazole), 7.282 ( $\text{CDCl}_3$ ), 6.836–6.830 (d, 1H, pyrazole CH), 3.850 (s, 3H, pyrazole N– $\text{CH}_3$ ) [Supplementary Fig. S2].  $^{13}\text{CNMR}$  (100 MHz,  $\text{CDCl}_3$ )  $\delta$ : 160.43, 150.90, 149.11, 146.28, 146.02, 130.98, 126.59, 122.89, 97.29, 38.88 [Supplementary Fig. S3]; DEPT  $\delta$ : 149.11, 130.88, 126.59, 122.89, 97.29, 38.88 [Supplementary Fig. S4]. MS (LC-MS)  $m/z$  (% rel.): 237 [ $\text{M}+\text{H}^+$ ] (90.66), 239 (28.72), 259 [ $\text{M}+\text{Na}^+$ ] (100.00), 261 (35.85) [Supplementary Fig. S5]. Anal. Calcd for  $\text{C}_{10}\text{H}_9\text{N}_4\text{OCl}$ : C 50.75; H 3.83; N 23.67. Found: C 50.88; H 3.80; N 23.72.

The single crystals suitable for X-ray analysis were obtained by the slow evaporation method. A pure form of the L4 was dissolved in methylene chloride and kept undisturbed at 283 K. Single crystals of L4 were obtained in 3 weeks.

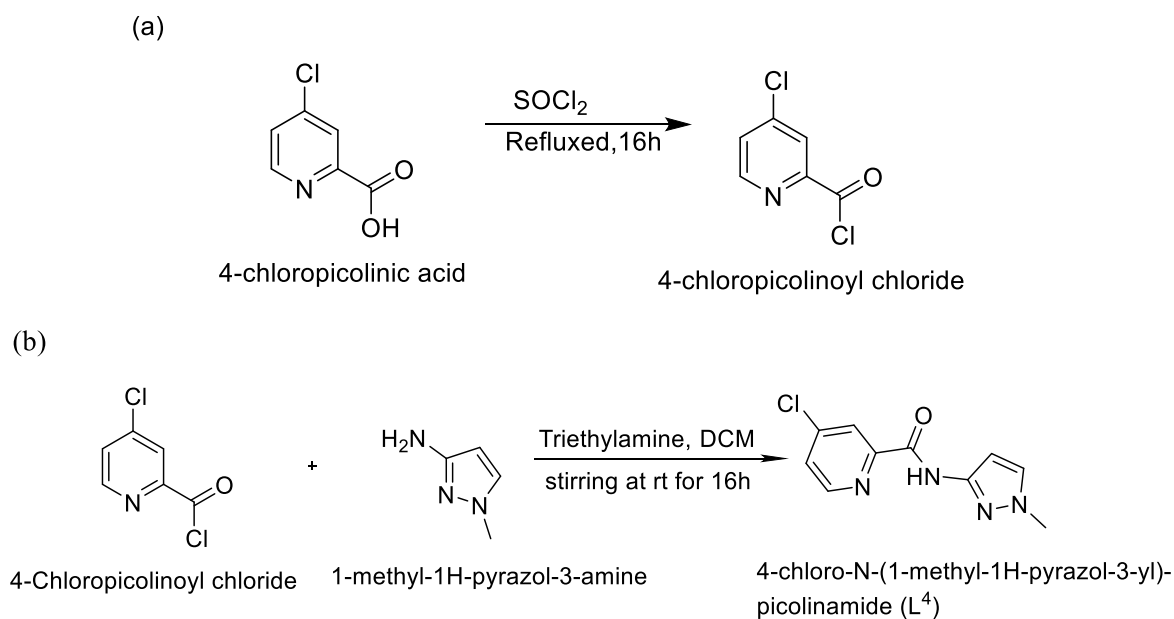


**Fig. 2:** (a) Synthesis of 4-chloropicolinoyl chloride; (b) Synthesis of 4-chloro-N-(1-methyl-1H-pyrazol-3-yl)picolinamide ( $\text{L}^4$ )

## Methods

### Separation Methodology

For liquid-liquid biphasic separation, 1 mg  $\text{mL}^{-1}$  of  $\text{Eu}^{3+}$  solution containing nitric acid of a specific concentration was taken as the aqueous phase. The organic phase contained 0.1 M ligand in 1-hexyl-

3-methylimidazolium NTf<sub>2</sub>. A 2.5 mL of organic and aqueous phases were taken in a separating funnel and allowed to equilibrate for 60 min unless otherwise mentioned. This 60 min was used for biphasic mass transfer. Then both phases were centrifuged for 5 min for complete phase separation. Subsequently, 2 mL aliquots were taken to determine Eu by EDXRF. The extraction was carried out at 300 K. For the acid variation experiment, the aqueous phase nitric acid concentration was varied from 0.01 M to 6 M HNO<sub>3</sub>, keeping all other experimental parameters constants. Whereas for ligand variation studies, the ligand concentration varied between 0.01 M and 0.4 M in the presence of 1M HNO<sub>3</sub> feed with Eu<sup>3+</sup> initial concentration of 1 mg mL<sup>-1</sup>. In the case of nitrate ion variation, the nitrate ion (NaNO<sub>3</sub>) in the aqueous phase varied from 0.1 M to 4 M, keeping the HNO<sub>3</sub> concentration 0.05 M. The ligand concentration was kept at 0.1 M in hexyl methyl imidazolium NTf<sub>2</sub>.

### ***Computational Methodology***

In this study, all the electronic structure calculations have been carried out in Turbomole-7.2 software.<sup>20</sup> The geometries of all the bare ligands and their europium nitrate complexes have been optimized without any symmetry restriction using density functional theory (DFT) based methods with Becke's three-parameter exchange and Lee–Yang–Parr correlation (B3LYP) functional with def-SV(P) basis set.<sup>21</sup> For the europium (Eu) atom, the effective core potential (ECP) has been included, where 28 electrons are considered in the core. In the Turbomole basis set library, the def-SV(P) basis set for Eu atom is quite large and consists of (14s13p10d8f1g) functions contracted to [10s8p5d4f1g]. The def-SV(P) basis sets used for the lighter elements and H, Cl, Br consist of (4s), (10s7p<sup>1</sup>d), (14s10p6d) functions contracted to [2s], [4s3p<sup>1</sup>d], [5s<sup>4</sup>p<sup>3</sup>d], respectively, while for C, N, O elements basis set contains (7s4p1d) functions contracted to [3s<sup>2</sup>p<sup>1</sup>d] as implemented in Turbomole.<sup>22</sup> To obtain the minimum energy structure, frequency calculation has been performed for all the systems using the same method. All the calculated real frequency values confirm the stability of the ligands' structures and their complexes with Eu<sup>3+</sup>. To study the effect of solvation in aqueous and ionic liquid phases, single point energy calculations have been carried out for the bare ligands and all the complexes to mimic the aqueous and ionic liquid phases ( $\epsilon = 78.4$  and  $12.5$  for the aqueous and ionic liquid phases, respectively) using the conductor like screening model (COSMO).<sup>22</sup> The atomic radius values used in the COSMO model are 1.300, 2.000, 1.830, 1.720, 2.050, and 2.223 Å for H, C, N, O, Cl, and Eu, respectively.<sup>23</sup> In addition, the quantum theory of atoms-in-molecule (QTAIM)<sup>24</sup> as developed by Bader has been adopted for quantitative estimation of the nature of the Eu–O and Eu–N chemical bonding using B3LYP method with def-SV(P) basis set by employing the Multiwfn<sup>25</sup> program for the bond critical point (BCP) properties. The partial atomic charges have been computed using the natural

population analysis (NPA) scheme at B3LYP/def-SV(P) level of theory as implemented in Turbomole. Energy decomposition analysis (EDA)<sup>26</sup> has been proven as an important tool to explore the nature of bonding in different bound systems. Accordingly, EDA has been carried out considering scalar relativistic effects for the heavier atom (Eu) using the zeroth-order regular approximation (ZORA) approach by employing B3LYP-D3/TZ2P method using the ADF (2017) program package.<sup>27</sup> In the EDA method, the total interaction energy between the considered fragments has been decomposed into four energy terms, viz., Pauli repulsion ( $\Delta E^{\text{Pauli}}$ ), electrostatic interaction ( $\Delta E^{\text{elstat}}$ ), orbital interaction ( $\Delta E^{\text{orb}}$ ), and dispersion interaction ( $\Delta E^{\text{disp}}$ ) and is correspondingly described as,

$$\Delta E^{\text{int}} = \Delta E^{\text{Pauli}} + \Delta E^{\text{elstat}} + \Delta E^{\text{orb}} + \Delta E^{\text{disp}} \quad (1)$$

## Results and Discussions

### *X-ray crystal structure*

Single-crystal XRD reveals that the ligand L<sup>4</sup> belongs to a monoclinic crystal system with space group P21/c having four molecules in the unit cell (Z=4, Figure 3). The determined lattice parameters are a = 5.663(16) Å, b = 9.196(2) Å, c = 20.664(5) Å,  $\alpha = 90^\circ$ ,  $\beta = 95.218(9)^\circ$ ,  $\gamma = 90^\circ$ , and volume = 1071.5(5) Å<sup>3</sup>. The ligand's crystal structure data, experimental conditions, and structural refinement parameters are presented in **Table 1**. A few selected bond length and angle parameters are listed in Supplementary Table T1 and T2. The crystal data of the ligand L<sup>4</sup> (**Supplementary Table T1, T2 and Figure 3**) shows that the molecule is not planar. The aromatic chlorine bond length viz. C(1)–Cl(1) of 1.738 Å is similar to those seen in the related structures 4-chloropyridine-2-carbonitrile (1.740 Å)<sup>28</sup> and 4-chloropyridine hydrochloride (1.730 Å)<sup>28,29</sup>. The pyridine ring C(3)–N(1) and C(5)–N(1) bond lengths of 1.335 Å and 1.336 Å are similar to those found in 4-chloropyridine-2-carbonitrile (1.350 and 1.361 Å respectively)<sup>28</sup>. The average pyridine ring C–C bond lengths are 1.377 Å, which is very close to the 1.403 Å reported for 4-chloropyridine-2-carbonitrile<sup>28</sup>. The bond lengths for the amide group O(1)–C(6) and N(2)–C(6) are 1.216 and 1.346 Å, which are very close to those in the reported compound 2-Pyridinecarboxamide (1.253 and 1.317 Å respectively)<sup>30</sup>. The bond angles C(2)–C(1)–Cl(1) and C(4)–C(1)–Cl(1) are not the same, and the value is 120.19° and 119.49°, respectively. The bond angles at the C=O carbon of amide group are O(1)–C(6)–N(2) = 124.84(14)°, O(1)–C(6)–C(5) = 121.80(14)° and N(2)–C(6)–C(5) = 113.35(12)°. These values suggest that bond angles deviate from the typical sp<sup>2</sup> bond angle, causing planarity loss in the molecule. Supplementary Fig. S6 depicts the crystal packing along a, b and c axis of of 4-Chloro-N-(1-methyl-1H-pyrazol-3-yl)-picolinamide (L<sup>4</sup>)



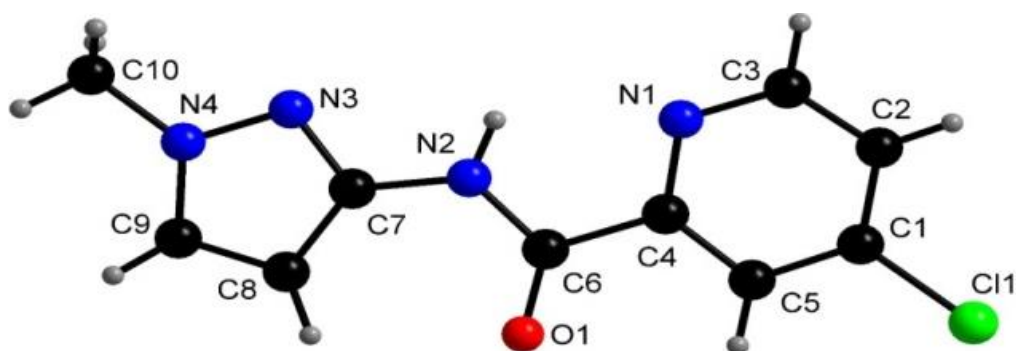


**Fig.3:** Asymmetric unit of 4-Chloro-N-(1-methyl-1H-pyrazol-3-yl)-picolinamide ( $L^4$ ) single crystal XRD structure.

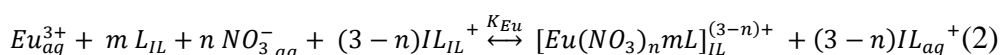
**Table 1.** Crystallographic data and structure refinement summary for 4-Chloro-N-(1-methyl-1H-pyrazol-3-yl)-picolinamide ( $L^4$ )

Identification code	shelx	
Empirical formula	$C_{10} H_9 Cl N_4 O$	
Formula weight	236.66	
Temperature	296(2) K	
Wavelength	0.71073 Å	(f)
Crystal system	Monoclinic	
Space group	P 21/c	
Unit cell dimensions	$a = 5.6626(16)$ Å	$\alpha = 90^\circ$ .
	$b = 9.196(2)$ Å	$\beta = 95.218(9)^\circ$ .
	$c = 20.664(5)$ Å	$\gamma = 90^\circ$ .
Volume	$1071.5(5)$ Å <sup>3</sup>	
Z	4	
Density (calculated)	1.467 Mg/m <sup>3</sup>	
Absorption coefficient	0.340 mm <sup>-1</sup>	
F(000)	488	
Crystal size	0.5 x 0.4 x 0.3 mm <sup>3</sup>	
Theta range for data collection	2.971 to 28.439°.	
Index ranges	-7 ≤ h ≤ 7, -12 ≤ k ≤ 12, -27 ≤ l ≤ 27	
Reflections collected	15256	
Independent reflections	2694 [R(int) = 0.0336]	
Completeness to theta = 25.242°	99.5%	
Absorption correction	Semi-empirical from equivalents	
Refinement method	Full-matrix least-squares on F <sup>2</sup>	
Data / restraints / parameters	2694 / 0 / 146	
Goodness-of-fit on F <sup>2</sup>	1.038	
Final R indices [I > 2σ(I)]	R1 = 0.0404, wR2 = 0.0951	
R indices (all data)	R1 = 0.0513, wR2 = 0.1010	
Extinction coefficient	n/a	
Largest diff. peak and hole	0.208 and -0.208 e.Å <sup>-3</sup>	
<b>CCDC No.</b>	<b>2205776</b>	

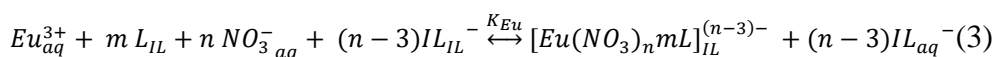
### *Liquid-liquid biphasic mass transfer*

The  $D_{Eu}$  values follow the trend  $L^4 > L^3 > L^2 > L^1$  [Fig. 4(a)]. This trend demonstrates the feasibility of metal ions approaching the ligand for complex formation. The bulkiness of R in the amide group is in the order of  $L^1 > L^2 > L^3$ . The Connollysolvent excluded volume calculated for  $L^1$ ,  $L^2$  and  $L^3$  using PerkinElmer, Chem3D software is 98.5, 68.3 and  $58.6 \text{ \AA}^{30}$ , respectively. The larger volume of the R-group in the ligand may hinder the approach of metal ions, which restricts the complex formation. However,  $L^4$  is a monoamide having open access to metal ions from one side. So the metal ions can approach  $L^4$  much easier than other ligands such as  $L^1$ ,  $L^2$  and  $L^3$ . Furthermore, The  $D_{Eu}$  value decreases with an increase in the  $HNO_3$  concentration in the aqueous phase [Fig. 4(b)]. This trend is reversed compared to that observed for molecular diluents. Unlike molecular diluents, where the liquid-liquid biphasic mass transfer of metal ions using neutral ligand proceeds through a solvation mechanism involving neutral metal-ligand species<sup>31</sup>, an ion exchange mechanism is proposed to be operative in the present case<sup>32</sup>. However, further confirmation is required through detailed speciation. When the number of nitrate ions associated during complexation ( $n$ ) is less than the charge of  $Eu^{3+}$  ion, i.e.  $+3$ , the mass transfer will proceed through the cation exchange mechanism involving cationic species. The charge would be compensated by transferring the equivalent number of ionic liquid cations ( $IL^+$ ) from the ionic liquid phase to the aqueous phase. However, in the case of  $n > 3$ , the anion exchange mechanism would be predominant, involving an anionic metal-ligand-nitrate complex. This complex formation is associated with transferring ionic liquid anion ( $IL^-$ ) to the aqueous phase for charge compensation.

#### *Cation exchange Mechanism*



#### *Anion exchange Mechanism*



$K_{Eu}$  is the equilibrium constant for the biphasic mass transfer, and it can be expressed as

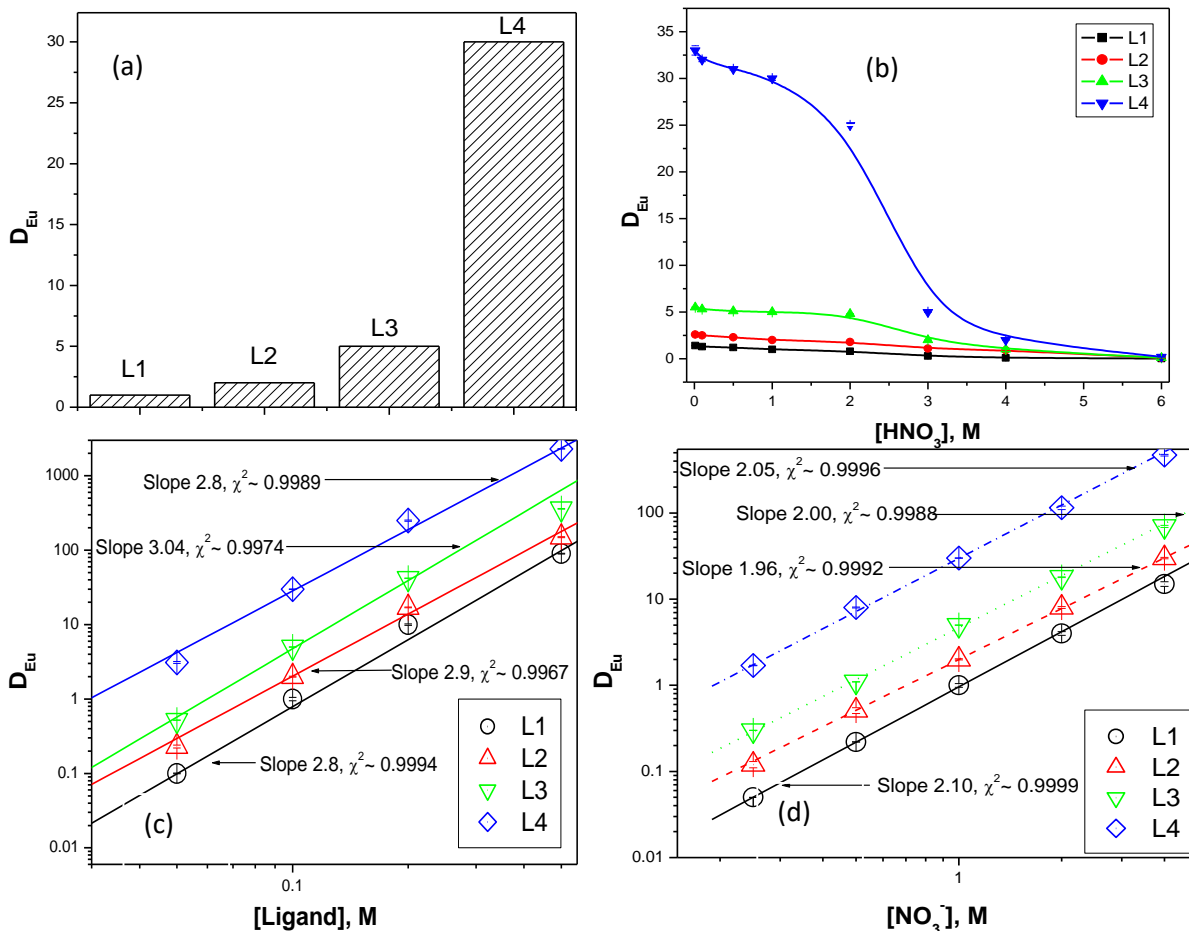
$$K_{Eu} = \frac{[Eu(NO_3)_n mL]_{IL}^{(3-n)+} [IL_{aq}^+]^{3-n}}{[Eu_{aq}^{3+}] [L_{IL}]^m [NO_3^-]_{aq}^n [IL_{IL}^+]^{3-n}} \quad (4)$$

$$K_{Eu} = \frac{[Eu(NO_3)_n mL]_{IL}^{(n-3)-} [IL_{aq}^-]^{n-3}}{[Eu_{aq}^{3+}] [L_{IL}]^m [NO_3^-]_{aq}^n [IL_{IL}^-]^{n-3}} \quad (5)$$

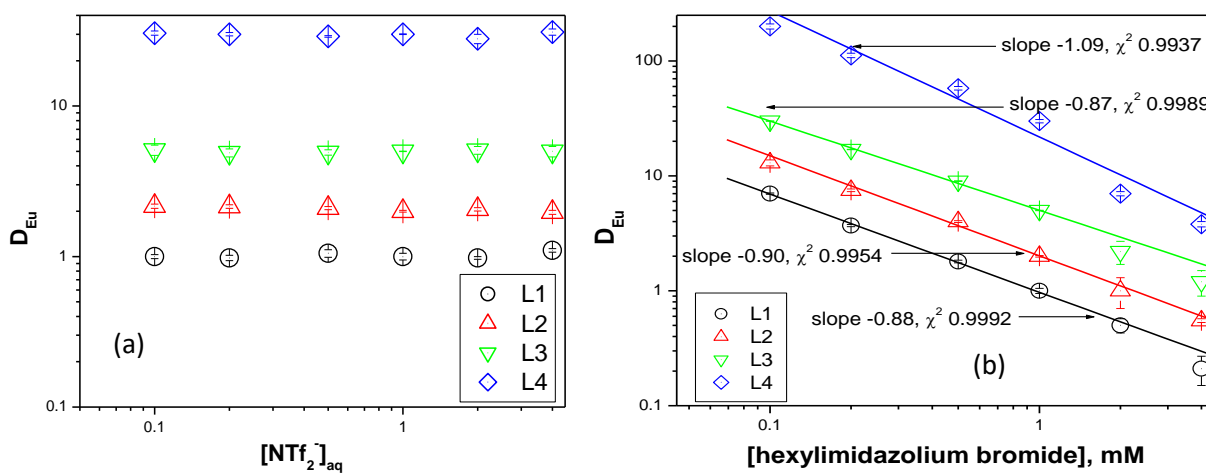
At a particular temperature and experimental condition, the distribution of  $IL^+$  and  $IL^-$  in both phases would maintain a constant ratio depending on the partition function of the constituent ions. The distribution ratio for Eu ( $D_{Eu}$ ) can be expressed in terms of the ratio of the analytical concentration of  $Eu^{3+}$  ions in ionic liquid and aqueous phase. Therefore, the equations can be simplified to equation 6 after taking the log on both sides and mathematical rearrangement.

$$\log D_{Eu} = \log K'_{Eu} + m \log [L]_{IL} + n \log [NO_3^-]_{aq} \quad (6)$$

Based on the above equation, a log-log plot between  $D_{Eu}$  and ligand concentration has a linear dependence, with a slope that estimates the number of ligand molecules associated with each  $Eu^{3+}$  ion (at a given aqueous feed acidity). Similarly, the number of nitrate ions associated with each  $Eu^{3+}$  ion can be estimated at a particular ligand concentration. **Fig. 4(c)** depicts the variation of  $\log D_{Eu}$  as a function of  $\log[\text{ligand}]$  concentration. The biphasic mass transfer was performed with 1 M  $HNO_3$ . The slope for the linear regression analysis was 2.8 ( $\chi^2 \sim 0.9994$ ), 2.9 ( $\chi^2 \sim 0.9967$ ), 3.04 ( $\chi^2 \sim 0.9974$ ) and 2.8 ( $\chi^2 \sim 0.9989$ ) for  $L^1$ ,  $L^2$ ,  $L^3$ , and  $L^4$ , respectively. This indicates the formation of  $ML_3$  type of complex for all the ligands. **Fig. 4(d)** shows the dependence of  $D_{Eu}$  as a function of nitrate ion concentration in the aqueous phase at 0.1 M ligand concentration. The slope evaluated from the linear regression analysis is 2.10 ( $\chi^2 \sim 0.9999$ ), 1.96 ( $\chi^2 \sim 0.9992$ ), 2.00 ( $\chi^2 \sim 0.9988$ ) and 2.05 ( $\chi^2 \sim 0.9996$ ), for the ligands ( $L^{1-4}$ ) respectively, revealing the participation of two nitrate ions with each  $Eu^{3+}$  ion during the biphasic extractive mass transfer. The above studies propose that the speciation is  $[Eu(NO_3)_2L_3]^+$ . Therefore, the cation exchange mechanism is predominantly operative. The charge compensation would be done by transferring one imidazolium cation from the ionic liquid phase to the aqueous phase in exchange for each  $Eu^{3+}$ -L complex. The Karl Fischer analysis and acid-base titration revealed that the ionic liquid after pre-equilibration with 1 M  $HNO_3$  was found to contain 1.6 % of water with 0.01 M  $HNO_3$ , respectively.



**Fig.4:** (a) The  $D_{Eu}$  values for different amide ligands; (b) variation in  $D_{Eu}$  values as a function of nitrate ion concentration in the aqueous phase; (c) variation in  $D_{Eu}$  as a function of ligand concentration; (d) variation in  $D_{Eu}$  as a function of nitrate ion concentration in the aqueous phase



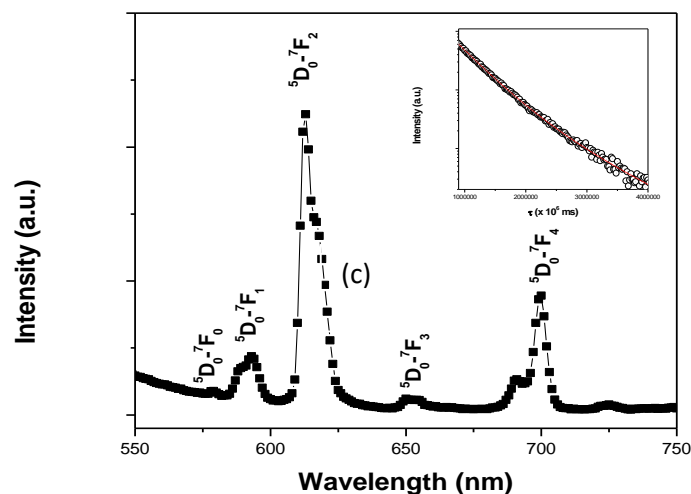


**Fig.5:** (a) Variation in  $D_{Eu}$  value as a function of  $NTf_2^-$  ion and (b) hexyl imidazolium cation concentration in the aqueous phase; (c) Luminescence spectra with lifetime for  $Eu^{3+}$ - $L^4$  complex

**Fig. 5(a)** depicts the variation in  $D_{Eu}$  values as a function of  $NTf_2^-$  ion concentration in the aqueous phase. The  $NTf_2^-$  ion in the aqueous phase was introduced by means of  $LiNTf_2$  salt. It was observed that the  $D_{Eu}$  value was independent of the  $[NTf_2^-]$  concentration suggesting that  $NTf_2^-$  ion is not directly participating in the biphasic mass transfer of  $Eu^{3+}$ . This result suggests that the biphasic mass transfer does not involve anionic moieties, i.e. the mass transfer does not involve an anion exchange mechanism. This result is in accordance with the speciation studies. **Fig. 5 (b)** shows the variation of  $D_{Eu}$  as a function of hexyl methylimidazolium cation in the aqueous phase. 1-Hexyl-3-methylimidazolium bromide was the source for the cations in the aqueous phase. It is evident from Fig. 5b that, the  $D_{Eu}$  values decrease with an increase in hexyl methylimidazolium cation in the aqueous phase. This result suggests that hexyl methylimidazolium cation in the aqueous phase would drive the phase transfer equilibrium in the backward direction. This finding corroborates the formation of a cationic complex. The slopes were found to be  $-0.88$  ( $\chi^2 \sim 0.9992$ ),  $-0.90$  ( $\chi^2 \sim 0.9954$ ),  $-0.87$  ( $\chi^2 \sim 0.9989$ ), and  $1.09$  ( $\chi^2 \sim 0.9937$ ) for these amide ligands respectively. This revealed the formation of mono-positive Eu complex ( $[EuL_3(NO_3)_2]^+$ ) during extractive mass transfer. Consequently, one hexyl methylimidazolium ion from the ionic liquid phase would transfer to the aqueous phase to keep charge neutrality. Fig. 5 (c) is depicting the photo luminescence spectra and decay profile for the excited species of  $Eu^{3+}$ - $L^4$  complex.  $L^4$  showed maximum extraction of  $Eu^{3+}$  and hence chosen for photoluminescence investigation. The peak at  $\sim 578$  nm and  $\sim 592$  nm were ascribed to  $^5D_0$ - $^7F_0$  and  $^5D_0$ - $^7F_1$  transitions, respectively. The later transition is magnetic dipole transition and hence do not perturb

by ligand field.<sup>33</sup> However, peak at ~613 nm and 652 nm were ascribed to electric dipole transitions assigned as  $^5D_0-^7F_2$  and  $^5D_0-^7F_3$  transitions, respectively. The former transition was highly sensitive to ligand field symmetry. The ratio of the peak intensity correspond to  $^5D_0-^7F_2$  transition to  $^5D_0-^7F_1$  transition was termed as asymmetry factor and was found to be 2.11 in the present case, revealing highly asymmetric environment around  $Eu^{3+}$  ion with respect to centre of symmetry<sup>34</sup>. The peak ~ 697 nm was ascribed to  $^5D_0-^7F_4$  transition. The mono-exponential decay profile indicated the presence of single species, while the lifetime value was used to calculate the number of inner sphere water molecules associated to the  $Eu^{3+}$  ion using empirical formula reported elsewhere<sup>35</sup>. For  $Eu^{3+}-L^4$  complex it was found to be 1, i.e. one water molecule was associated to the  $Eu^{3+}$  in its primary coordination sphere. The photoluminescence spectra for other  $Eu^{3+}$  complexes were shown in **Supplementary Fig. S7**. The life time data for these  $Eu^{3+}$  complexes were found to be 1.24 ms, and 1.33 ms for  $L^1$  and  $L^2$ , respectively. It revealed that, these complexes did not possess any inner sphere water molecule in the primary coordination sphere of  $Eu^{3+}$ . However, the  $L^3$  and  $L^4$  complexes were found to have one water molecule in the primary coordination sphere of  $Eu^{3+}$  ion as suggested from the life time of their excited species ( $\tau_{L3} \sim 680 \mu s$  and  $\tau_{L4} \sim 704 \mu s$ , respectively).

$L^3$  and  $L^4$  only showed measurable extraction of  $Eu^{3+}$  and hence our further discussion would mostly be centred around these two ligands. Fig. 4 (b): showing the  $D_{Eu}$  values decreased with increase in aqueous phase acidity. This trend is an indication of predominance of cation exchange mechanism. This trend is well supported by literatures on separation of f-block element cations into ionic liquid based systems using different extractants<sup>36</sup>. Fig. 4(c): The slope values revealed the formation of  $ML_3$  type of complexes by  $Eu^{3+}$  with all the ligands in ionic liquid. Since ligands are neutral in nature and hence do not play any role in deciding the overall charge of the metal-ligand complex. Fig. 4(d): The slope values revealed the formation of 1:2 M- $NO_3$  complex, i.e. per  $Eu^{3+}$  ion, two nitrate ion is involved for the formation of complex. Since  $Eu^{3+}$  is having tripositive charge and each nitrate ion is mono negative charge, then the overall charge is mono positive for the Eu complex (unless other species are also involved),  $[EuL_3(NO_3)_2]^+$ . Fig. 5 (a) and Fig 5 (b) are different types of experiments to confirm the cation exchange mechanism and the species  $EuL_3(NO_3)_2^+$ . Le Chatelier's principle on chemical equilibrium has been utilized in these two experiments. Fig.5(a) is demonstrating that even if the water phase during extraction is contaminated with variety of concentrations of  $NTf_2^-$  ion, the D values are insensitive to it. This indicated that  $NTf_2^-$  anion is not participating in formation of metal-ligand complex either directly or indirectly. This rules out the existence of 'anion exchange' mechanism during liquid-liquid biphasic mass transfer. Fig. 5 (b) provides very useful information and confirmative to the speciation claimed. Here, the ionic liquid cation has been dissolved in aqueous phase at various

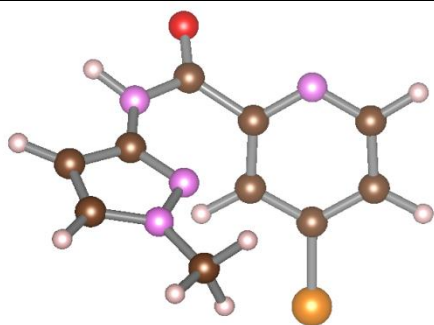
concentration followed by extraction. The mono negative slope (-1) straight line clearly revealed that, presence of  $C_6mim^+$  in aqueous phase put hurdle in moving the extraction equilibrium towards forward direction. This is only possible if the  $C_6mim^+$  is getting exchanged from ionic liquid phase to water during extraction. The -1 slope also revealed that only one  $C_6mim^+$  is getting exchanged during extraction of each Eu complex.

This analogy has been exploited several time in literature in ascertaining the speciation and extraction mechanism<sup>9,10</sup> and hence also followed in the present case.

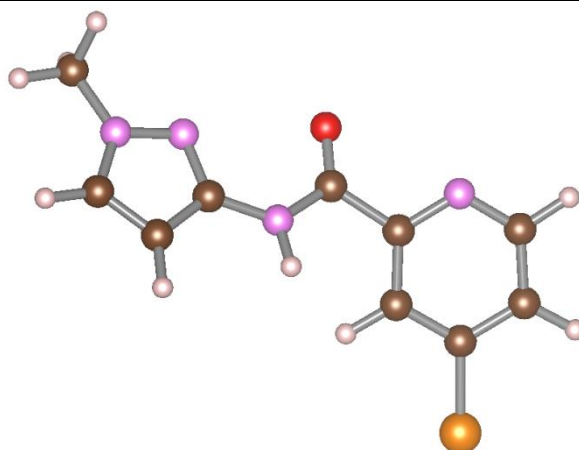
### ***Theoretical Studies***

In addition to the experimental results, we have also theoretically investigated the structure, stability, and bonding analysis of the experimentally synthesized compounds. For this purpose, geometry optimizations have been carried out for all the synthesized bare ligands, *viz.*,  $L^1$ ,  $L^2$ ,  $L^3$ , and  $L^4$  as well as the complexes of Eu(III) with the ligand ( $L^4$ ) to obtain the minima energy structures in their ground electronic state. Since the size of the ligands ( $L^1$ ,  $L^2$ , and  $L^3$ ) are quite large and the experimental findings indicate the formation of Eu(III)-complexes involving three ligands for each cases as evident from the experimental results, it has not been possible to optimize the structures theoretically by accommodating three ligands ( $L^1$  or  $L^2$  or  $L^3$ ) surrounding the metal ion. Therefore, we have restricted our discussions with the all possible geometrical isomers of the bare ligand ( $L^4$ ) and its complexes with the  $Eu^{3+}$  ion.

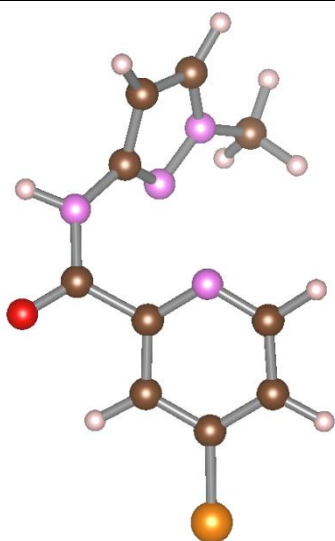
The optimized structures of all the synthesized bare ligands, *viz.*,  $L^1$ ,  $L^2$ , and  $L^3$  are shown in **Supplementary Fig. S8** as obtained by using B3LYP method and def-SV(P) basis set. Since the calculations have been carried out for the Eu(III) complexes with the  $L^4$  extractant, therefore, we have considered all possible isomers of the ligand ( $L^4$ ). Ligand ( $L^4$ ) has 4 pairs of geometrical isomers whose B3LYP/def-SV(P) optimized structures are depicted in Fig. 6. From the Fig.6, it is evident that *trans*-isomer (T4) is found to be most stable among all possible *cis*- and *trans*-isomers of the bare ligand ( $L^4$ ).



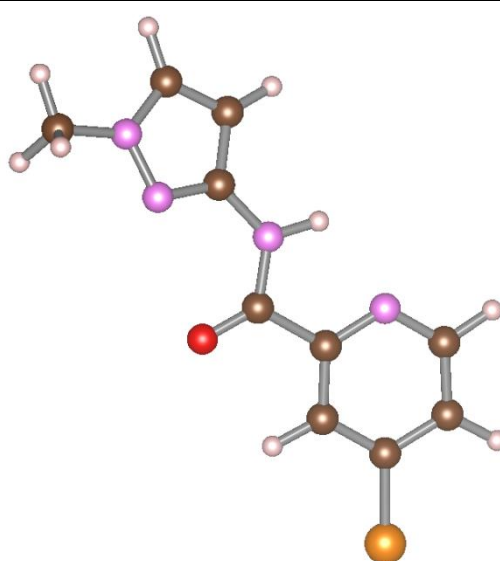
*cis*-L4 (C1) [15.9]



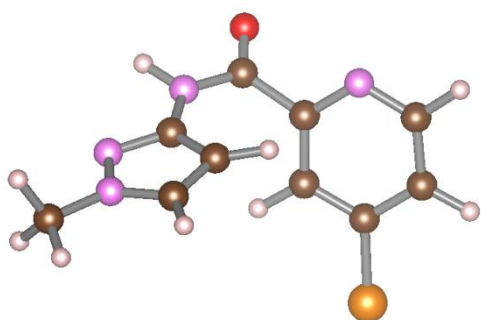
*trans*-L4 (T1) [16.9]



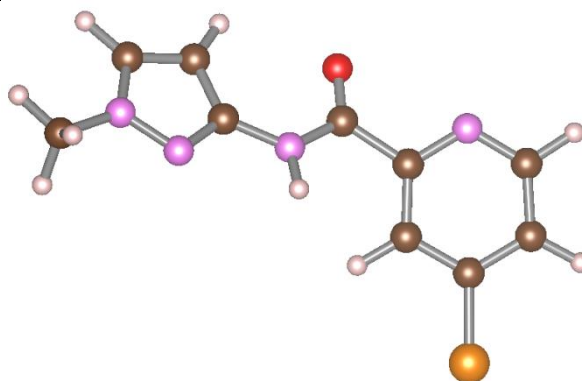
*cis*-L4 (C2) [12.5]



*trans*-L4 (T2) [5.9]



*cis*-L4 (C3) [14.8]



*trans*-L4 (T3) [9.9]



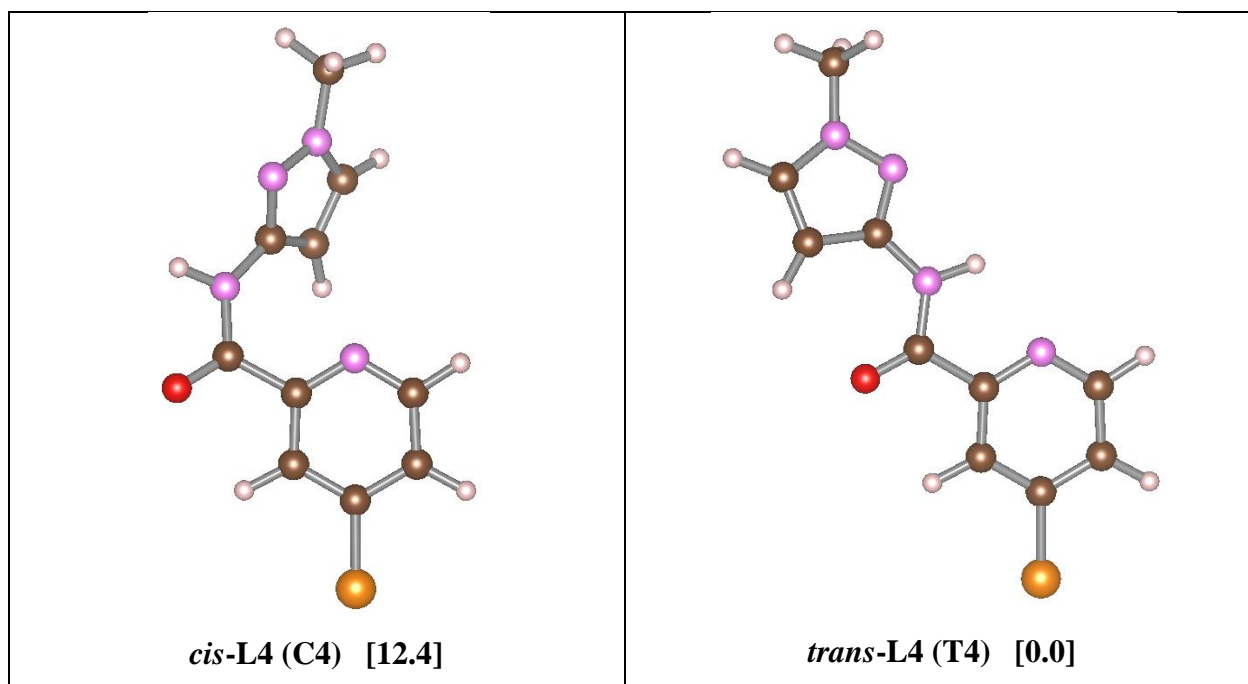
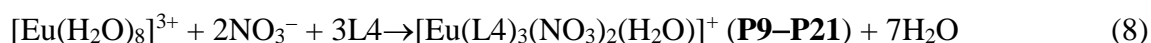


**Fig.6.** Optimized structures of all possible *cis*-isomers of Ligand-4 ( $L^4$ ), *viz.*, C1, C2, C3, C4 and *trans*-isomers of Ligand-4 ( $L^4$ ), *viz.*, T1, T2, T3, T4 as obtained by using B3LYP method and def-SV(P) basis set. The white, dark green, pink, red, and saffron represent H, C, N, O, and Cl atoms, respectively. Relative energy values (in kcal mol<sup>-1</sup>) are provided in the square brackets.

In this context, it is to be mentioned that Dolg and his co-workers<sup>37-39</sup> have made an exhaustive study to investigate the hydration of lanthanide(III) theoretically and concluded that the preferred hydration number is 8 in Eu(III) which is also supported by some other group of scientists<sup>40-42</sup>. They have also reported that the *octa*-aquo complexes are favored in lanthanoid(III) hydration complexes while actinide ( $An^{3+}$ ) ions slightly preferred to form *nona*-aquo complexes<sup>43</sup>. Although  $Eu^{3+}$  ion form 8 coordinated hydrated complex, *i.e.*,  $[Eu(H_2O)_8]^{3+}$ , 9 and 10 coordination sites of  $Eu^{3+}$  can also be occupied by mono- and multi-dentate neutral or anionic ligands forming various 8-10 coordinate Eu(III) complexes. In addition to the 8 and 9 coordinate Eu(III) complexes<sup>44-46</sup>, the coordination number of 10 have also been reported in several Eu(III) complexes<sup>47-49</sup>. It is to be noted that the Eu(III) form cationic complexes with the neutral multi-dentate ligands with coordination number 10 as reported by Paschalidis<sup>50</sup>. Therefore, we have considered all possible isomers of the Eu(III) complexes with all the geometrical isomers of  $L^4$  along with the variable positions of  $NO_3^-$  and  $H_2O$  ligands surrounding the metal ion. All plausible coordination number of 8 to 10 have been investigated for the Eu(III) complexes where all probable coordination sites of the ligand ( $L^4$ ), *viz.*, N-pyridine, N-

pyrazole, and O-amide with mono- or/and bi-dentate behavior of all the isomers of L<sup>4</sup> and NO<sub>3</sub><sup>-</sup> along with/without an additional H<sub>2</sub>O ligand have been taken into account.

An extensive calculations have been carried out and found 21 stable Eu(III) complexes (P1–P21) possessing 8-10 coordination sites. The optimized structures of all these 21 complexes have been depicted in Supplementary **Supplementary Fig.S9**. As shown in **Supplementary Fig.S9**, the H<sub>2</sub>O acts as a ligand in the P9–P21 complexes while P1–P8 complexes contain no H<sub>2</sub>O ligand. As reported by Dolg and co-workers,<sup>37-39</sup> DFT calculated exchange energy did not reproduce the variation of hydration coordination number for the lanthanide series in between [Ln<sup>III</sup>(H<sub>2</sub>O)<sub>n</sub>]<sup>3+</sup> and [Ln<sup>III</sup>(H<sub>2</sub>O)<sub>n-1</sub>·H<sub>2</sub>O]<sup>3+</sup> complexes (*n* = 8, 9) where (*n*–1) molecules in the first hydration and 1 water molecule in the second hydration shell. They have also reported that the pure-GGA (Generalized Gradient Approximation), hybrid-GGA based DFT methods and second order Møller–Plesset perturbation theory (MP2) predict the preferred hydration number 8 for the Eu(III) which is in good agreement with the experimental results<sup>42</sup>. Therefore, we have calculated the all the thermodynamic properties of the products (P1–P21) based on the hydration coordination number 8 (CN = 8) of Eu(III), [Eu(H<sub>2</sub>O)<sub>8</sub>]<sup>3+</sup>. The most probable reactions that lead to the formation of the present studied Eu<sup>3+</sup>–ligand complexes (P1–P21) have been shown in the following equations (eqn.7 and eqn.8).



The complexation energies ( $\Delta E$ ) have been evaluated by using the following eqn.9 and eqn.10 for the abovementioned reaction pathways eqn.7 and eqn.8, respectively.

$$\Delta E = E\{[\text{Eu}(\text{L4})_3(\text{NO}_3)_2]^+\} + 8 E\{\text{H}_2\text{O}\} - E\{[\text{Eu}(\text{H}_2\text{O})_8]^{3+}\} - 2 E\{(\text{NO}_3)^-\} - 3 E\{\text{L4}\} \quad (9)$$

$$\Delta E = E\{[\text{Eu}(\text{L4})_3(\text{NO}_3)_2(\text{H}_2\text{O})]^+\} + 7 E\{\text{H}_2\text{O}\} - E\{[\text{Eu}(\text{H}_2\text{O})_8]^{3+}\} - 2 E\{(\text{NO}_3)^-\} - 3 E\{\text{L4}\} \quad (10)$$

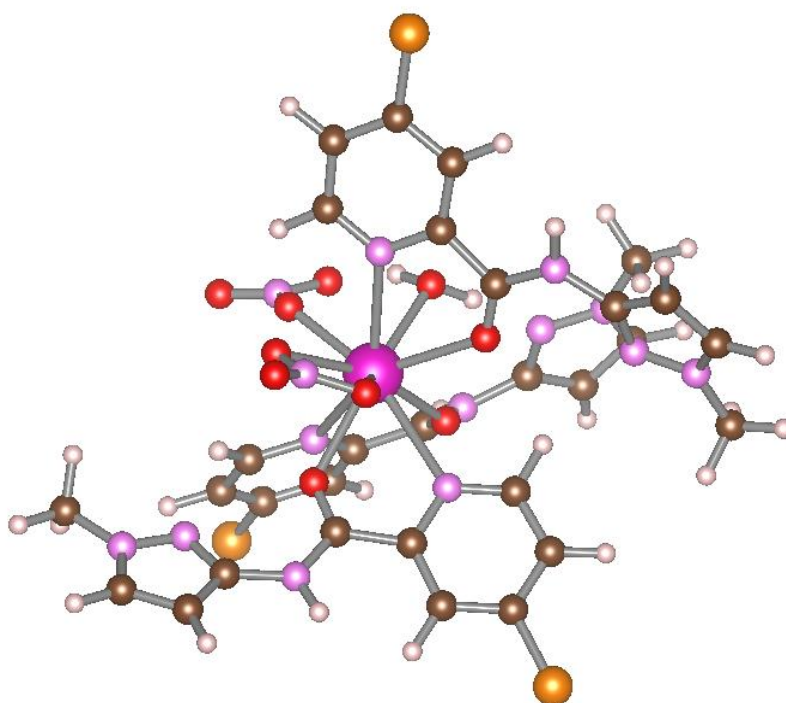
**Table 2.** Calculated Values of Complexation Energies ( $\Delta E_g$  in kcal mol<sup>-1</sup>), Solvation Energies ( $\Delta E_{sol}$  in kcal mol<sup>-1</sup>), Change in Enthalpies ( $\Delta H$  in kcal mol<sup>-1</sup>) and change in Gibb's Free Energies ( $\Delta G$  in kcal mol<sup>-1</sup>) in the Gas Phase (g) and Solvent Phase (sol) for the Proposed Reactions for all the Products (P1–P21) by using B3LYP Method with def-SV(P) Basis Set.

Reaction Channel No. 7						
Complex	$\Delta E_g$	$\Delta H_g$	$\Delta G_g$	$\Delta E_{sol}$	$\Delta H_{sol}$	$\Delta G_{sol}$
P1	-443.6	-450.1	-460.7	-53.9	-7.6	-18.1
P2	-437.9	-443.8	-458.8	-51.9	0.8	-14.2
P3	-439.7	-446.4	-459.6	-52.3	-2.1	-15.4
P4	-440.3	-446.0	-457.2	-46.6	3.9	-7.3
P5	-447.4	-453.5	-463.1	-48.3	-5.3	-14.9
P6	-434.1	-441.0	-456.7	-52.2	-5.6	-21.3
P7	-432.5	-438.8	-458.0	-51.6	-2.8	-22.0
P8	-431.0	-437.9	-454.1	-53.4	-3.6	-19.9
Reaction Channel No. 8						
Complex	$\Delta E_g$	$\Delta H_g$	$\Delta G_g$	$\Delta E_{sol}$	$\Delta H_{sol}$	$\Delta G_{sol}$
P9	-465.9	-456.2	-470.8	-53.7	-5.6	-20.2
P10	-465.8	-457.0	-469.6	-53.3	-6.2	-18.8
P11	-464.1	-455.2	-469.0	-51.6	-2.7	-16.4
P12	-457.2	-461.3	-463.7	-48.0	-5.1	-7.6
P13	-469.7	-473.3	-472.5	-48.6	-17.8	-17.0
P14	-462.9	-466.4	-466.2	-49.8	-12.1	-11.9
P15	-471.6	-475.3	-473.0	-48.2	-19.4	-17.0
P16	-451.8	-457.0	-456.9	-44.1	-8.3	-8.3
P17	-458.1	-462.5	-466.4	-43.3	-13.1	-16.9
P18	-450.7	-455.8	-459.9	-53.9	-14.4	-18.6
P19	-449.3	-454.6	-459.9	-51.8	-11.1	-16.5
P20	-453.9	-458.3	-464.0	-48.2	-11.2	-16.9
P21	-433.9	-439.1	-448.5	-42.8	4.0	-5.4

The negative values of the complexation energies ( $\Delta E_g$  as listed in Table 2) for both the reaction channels (7 and 8) indicate the exoergic nature of the paths leading to the formation of all the P1–P21 complexes. To understand the effect of solvation, the energies ( $\Delta E_{sol}$ ) of ( $\text{NO}_3^-$ ,  $\text{H}_2\text{O}$ ,  $[\text{Eu}(\text{H}_2\text{O})_8]^{3+}$ ) and ( $\text{L}^4$ , P1–P21) have been also calculated in aqueous ( $\epsilon = 78.4$ ) and in ionic liquids ( $\epsilon = 12.5$ ), respectively, and the results are tabulated in Table 2. The complexation energies ( $\Delta E_{sol}$ ) are found to

be in the range of  $-42.8$  to  $-53.9$  kcal mol<sup>-1</sup> in the solvents for formation of all the P1–P21 complexes. In order to compare the thermodynamic parameters related to the synthesis of all the P1–P21 complexes, the change in reaction enthalpy ( $\Delta H$ ) and change in Gibb's free energy ( $\Delta G$ ) for their corresponding formation reactions (eqn.7 and eqn.8) have been calculated in gas phase as well as in solvent phase and reported in Table 2. To mimic the actual experimental conditions, the free energy corrections and chemical potentials have been calculated at 298 K of temperature for all the reactants and products in gas phase corresponding to the channels 7 and 8. All the  $\Delta H$  and  $\Delta G$  values are found to be negative which in turn indicates that all the reactions are exothermic and spontaneous in nature in the gas phase. In contrast, the solvation enthalpy ( $\Delta H_{\text{sol}}$ ) values are found to be negative for all the products indicating the exothermic nature of the reaction (eqn.7 and eqn.8) except in case of P2, P4, and P21 complexes which show endothermic reaction pathways. On the other hand, both the channels are spontaneous in nature with negative values of  $\Delta G_{\text{sol}}$  as listed in Table 2 for all the Eu(III) complexes (P1–P21). Although the reaction channel 7 (P2 and P4) and 8 (P21) are endothermic in nature, they are spontaneous by virtue of the large amount of change in entropy, called as entropically controlled reaction. Among these 21 complexes, P6, P7, and P9 are found to be energetically favorable with larger negative values of change in free energy ( $\Delta G$ ). P6 and P7 contain no water molecule as ligand while P9 consists of one H<sub>2</sub>O as a ligand. In this context, it is to be noted that we have provided the Luminescence spectra of the synthesized Eu(III) complexes in the Fig.SX–SY (ESI<sup>†</sup>) which clearly indicate the existence of  $[\text{Eu}(\text{L})_3(\text{NO}_3)_2(\text{H}_2\text{O})_n]^+$  ( $n = 0$  for L<sup>1</sup> and L<sup>2</sup>;  $n = 1$  for L<sup>3</sup> and L<sup>4</sup>) complexes. Although the  $\Delta G$  values associated with the products follows the order  $\Delta G_{\text{P7}} < \Delta G_{\text{P6}} < \Delta G_{\text{P9}}$ , we have discussed P9 in detail throughout the text since the Luminescence spectra of the synthesized complex indicates the existence of one H<sub>2</sub>O as ligand along with three L<sup>4</sup> and two NO<sub>3</sub><sup>-</sup> ligands. Hence, in the present study, the Eu<sup>3+</sup> ion form most stable 10 coordinate  $[\text{Eu}(\text{T1})_3(\text{NO}_3)_2(\text{H}_2\text{O})]^+$  complex with the T1 isomer of the ligand (L<sup>4</sup>) where three T1 and one NO<sub>3</sub><sup>-</sup> act as bidentate ligands while one NO<sub>3</sub><sup>-</sup> and one H<sub>2</sub>O act as monodentate ligands. Moreover, it has been possible to characterize the Eu(III) complex with the L<sup>4</sup> ligand experimentally through NMR, FTIR, MS, or XRD techniques. Therefore, we have limited our discussions for the L<sup>4</sup> containing Eu(III) complexes leading to the formation of  $[\text{Eu}(\text{L}^4)_3(\text{NO}_3)_2]^+$  and  $[\text{Eu}(\text{L}^4)_3(\text{NO}_3)_2(\text{H}_2\text{O})]^+$  with all possible geometrical isomers of L<sup>4</sup> (Fig.6) which are abbreviated as (P1–P8) and (P9–P21), respectively. Herein, the optimized structural parameters, thermodynamic stability, partial charge distribution, AIM (atoms-in-molecule) analysis, and energy decomposition analysis (EDA) have been systematically reported for the most stable experimentally relevant P9 complex,  $[\text{Eu}(\text{T1})_3(\text{NO}_3)_2(\text{H}_2\text{O})]^+$ .

Fig.7 depicts the optimized structure of  $[\text{Eu}(\text{T1})_3(\text{NO}_3)_2(\text{H}_2\text{O})]^+$  (P9) complex as obtained by B3LYP/def-SV(P) level of theory. In P9 complex, *N*-donor of pyridine and *O*-donor of amide of T1 isomer of  $\text{L}^4$  ligand and *O*-donor of the  $\text{NO}_3^-$  and  $\text{H}_2\text{O}$  are the coordination sites for the  $\text{Eu}^{3+}$  metal ion (Fig.7). The B3LYP/def-SV(P) computed optimized structural parameters of P9 is reported in Table 3. Among all the  $\text{Eu}-\text{O}$  bonds, the average  $\text{Eu}-\text{O}_{\text{LIG}}$  bond distance is found to be larger than the corresponding  $\text{Eu}-\text{O}_{\text{NO}_3}$  by  $0.074 \text{ \AA}$  in the P9 complex. Therefore, it indicates that  $\text{Eu}^{3+}$  binds more strongly with the *O* atoms of the nitrate ligands as compared to that in the T1 ligand. Moreover, the interaction between the  $\text{Eu}^{3+}$  and *O* atom of nitrate is found to be stronger than that of the water which in turn stronger than that of the ligand (T1) as revealed from Table 3.



**P9**

**Fig.7.** Optimized structures of  $[\text{Eu}(\text{T1})_3(\text{NO}_3)_2(\text{H}_2\text{O})]^+$  (P9) as obtained by using B3LYP method and def-SV(P) basis set. The white, dark green, pink, red, saffron, and violet represent H, C, N, O, Cl, and Eu atoms, respectively.

**Table 3.** Optimized Structural Parameters, *viz.*, Average Eu–O Bond Length ( $R_{av(Eu-O)}$  in Å) and Eu–N Bond Length ( $R_{av(Eu-N)}$  in Å) for the P9 Complex by using B3LYP Method with def-SV(P) Basis Set.

Complexes	Selected Bond Distances			
	$R_{av(Eu-O)LIG}^a$	$R_{av(Eu-O)NO_3}^b$	$R_{av(Eu-O)H_2O}^c$	$R_{av(Eu-N)LIG}^d$
[Eu(T1) <sub>3</sub> (NO <sub>3</sub> ) <sub>2</sub> (H <sub>2</sub> O)] <sup>+</sup> ( <b>P9</b> )	2.514	2.440	2.496	2.766

<sup>a</sup> $R_{av(Eu-O)LIG}$ , <sup>b</sup> $R_{av(Eu-O)NO_3}$ , and <sup>c</sup> $R_{av(Eu-O)H_2O}$  indicate the average bond distances between Eu and O atoms of the ligand, nitrate, and water, respectively.

<sup>d</sup> $R_{av(Eu-N)LIG}$  represents the average bond distance between Eu and N atoms of the ligand.

In order to understand the nature of the Eu–O and Eu–N bonds in the P9 complex, we have calculated the partial charges on the donor as well as central Eu atom through the natural population analysis (NPA) using B3LYP method with def-SV(P) basis set and presented in Table 4. It is interesting to note that the charge on O and N atoms in the ligands (T1) and O atom in H<sub>2</sub>O is decreased by ~0.1 while the charge on O atom of NO<sub>3</sub><sup>−</sup> remain almost unaltered after complexation on going from precursor ligands to the product (P9). This signifies that there is charge redistribution on the donor atoms of the ligands before and after the complexation. Moreover, O-donor atoms belonging to T1 acquire more negative charge than that of the NO<sub>3</sub><sup>−</sup> which in turn more negative than the N donor atoms of the T1 in the P9 complex. Among all the donor atoms, the highest negative charge is residing on the O atom of H<sub>2</sub>O attached to the metal center. The higher negative charge possessed by the O-donor as compared to the N-donor in the P9 complex can be explained by higher electronegativity of the O atom than that of the N atom. In P9, the charge acquired by the Eu is found to be positive (1.663). The separation of charges are higher for Eu and O atoms in comparison to the Eu and N atom, which reveals that the Eu–N bond is found to be more covalent than that of the Eu–O bond in the P9 complex. Furthermore, the charge separation between the Eu and O<sub>LIG</sub> are more than that of the Eu and O<sub>NO<sub>3</sub></sub>, which emphasizes that higher non-covalent character persists on Eu–O<sub>LIG</sub> bond as compared to that in the Eu–O<sub>NO<sub>3</sub></sub> bond.

**Table 4.** Calculated Values of Average Partial Charges on Eu Atom ( $q_{Eu}$ ), O Atom ( $q_O$ ), N Atom ( $q_N$ ) Attached with Eu Atom in the P9 Complex using Natural Population Analysis (NPA) by employing B3LYP Method with def-SV(P) Basis Set.

Chemical Systems	NPA Charges on the Atoms				
	$q_{Eu}$	$q_{O(LIG)}^a$	$q_{O(NO_3)}^b$	$q_{O(H_2O)}^c$	$q_{N(LIG)}^d$
H <sub>2</sub> O	...	...	...	-0.864	...
NO <sub>3</sub> <sup>-</sup>	...	...	-0.577	...	...
T1	...	-0.552	...	...	-0.453
P9	1.663	-0.630	-0.551	-0.965	-0.499

<sup>a</sup> $q_{O(LIG)}$ , <sup>b</sup> $q_{O(NO_3)}$ , and <sup>c</sup> $q_{O(H_2O)}$  indicate the average partial atomic charges residing on O atoms of the ligand, nitrate, and water, respectively.

<sup>d</sup> $q_{N(LIG)}$  represents the average partial atomic charges on N atoms of the ligand

To determine the nature of Eu–O and Eu–N bonding in P9, we have carried out topological analysis of the electron densities involved in the corresponding bonds using Bader’s quantum theory of atoms-in-molecules (QTAIM).<sup>52</sup> Consequently, for Eu–O and Eu–N bonds in P9 complex, the electron density [ $\rho$ ], Laplacian of the electron density [ $\nabla^2\rho$ ], kinetic energy density [ $G$ ], potential energy density [ $V$ ], local energy density [ $E_d$ ], and the ratio between the kinetic energy density and the electron density [ $G/\rho$ ] at their bond critical points (BCPs) by employing DFT method have been calculated and reported in Table 5. Following the footsteps of Bogg’s and co-workers,<sup>53</sup> we have also categorized the covalent interactions existing in the above-mentioned bonds. As per the classification, the Eu–N bonds are of “Type D” covalent bonds satisfying the criteria [ $(G(r_c)/\rho(r_c) < 1$  and  $|E_d(r_c)| < 0.005$ ]. In contrast, the low value of electron density [ $\rho(r_c) < 0.1$ ] and positive values of  $\nabla^2\rho(r_c)$  and  $E_d(r_c)$  along with the criteria [ $(G(r_c)/\rho(r_c) > 1$ ] indicates that the Eu–O bond is of “W” category which infers the weak bonding interaction with some non-covalent (electrostatic) properties leading to the formation of ionic type Eu–O bond. Among all the Eu–O bonds, the lower values of  $E_d(r_c)$  and  $(G(r_c)/\rho(r_c))$  also emphasize that the Eu–O<sub>NO<sub>3</sub></sub> and Eu–O<sub>H<sub>2</sub>O</sub> bonds are less electrostatic as compared to the Eu–O<sub>LIG</sub> bonds. From the above discussion, it is clearly evident that the Eu–N bonds are associated with to some extent covalent character while the non-covalent ionic type electrostatic interaction is involved in Eu–O bonds in P9 complex. Therefore, the above AIM results are in concurrence with the NPA analysis.

**Table 5.** Calculated Values of Bond Critical Point Electron Density ( $\rho$  in  $e a_0^{-3}$ ), Laplacian ( $\nabla^2\rho$  in  $e a_0^{-5}$ ), the Local Electron Energy Density ( $E_d$  in au), and Ratio of Local Electron Kinetic Energy Density and Electron Density ( $G/\rho$  in au) in the P9 Complex as Obtained Using B3LYP Method with def-SV(P) Basis Set.

Complex	Bond	$\rho$	$\nabla^2\rho$	$G(r)^a$	$V(r)^b$	$E_d(r)$	$G(r)/\rho$	Type <sup>c</sup>
P9	<sup>d</sup> Eu–O <sub>LIG</sub>	0.034	0.175	0.038	–0.033	0.005	1.118	W <sup>n</sup>
	<sup>e</sup> Eu–O <sub>NO3</sub>	0.036	0.168	0.038	–0.035	0.004	1.056	W <sup>n</sup>
	<sup>f</sup> Eu–O <sub>H2O</sub>	0.035	0.167	0.038	–0.034	0.004	1.086	W <sup>n</sup>
	<sup>g</sup> Eu–N <sub>LIG</sub>	0.021	0.089	0.019	–0.016	0.003	0.905	D

<sup>a</sup> $G(r)$  represents the local electron kinetic energy density; <sup>b</sup> $V(r)$  signifies the local electron potential energy density; <sup>c</sup>“Type” is an indication of type of covalent bonding exists in between the corresponding pair of bonding atoms; <sup>d</sup>Eu–O<sub>LIG</sub>, <sup>e</sup>Eu–O<sub>NO3</sub>, and <sup>f</sup>Eu–O<sub>H2O</sub>, indicate the average BCP parameters for the Eu–O bonds where the O atoms belong to the ligand, nitrate, and water, respectively; <sup>g</sup>Eu–N<sub>LIG</sub> represents the average BCP parameters for the Eu–N bonds where the N atoms belong to the ligand.

To confirm the nature of bonding existing between the metal atom and the donor atoms, we have also performed the energy decomposition analysis (EDA), which is considered as a very effective tool for quantitative interpretation of chemical bonds in terms of three stabilizing (electrostatic, orbital, and dispersion) attraction and one destabilizing (Pauli) repulsion components. Table 6 lists the energy decomposition components like Pauli repulsion energy ( $\Delta E^{\text{Pauli}}$ ), electrostatic energy ( $\Delta E^{\text{elec}}$ ), orbital interaction energy ( $\Delta E^{\text{orb}}$ ), dispersion energy ( $\Delta E^{\text{disp}}$ ), and the total interaction energy ( $\Delta E^{\text{total}}$ ) for the dissociation into the seven fragments ( $\text{Eu}^{3+} + 3\text{Tl} + 2\text{NO}_3^- + \text{H}_2\text{O}$ ) for P9 complex, employing B3LYP-D3/TZ2P level of theory. From the Table 6, it is clearly evident that the contribution of electrostatic attraction is more towards the total interaction energy as compared to that of the orbital interaction. Here, the electrostatic interaction is found to be significant (73.5%) towards the total interaction energy while the orbital interaction contributes only 23.2% (Table 6). The total interaction energy ( $\Delta E^{\text{total}}$ ) has been found to be  $-1106.9 \text{ kcal mol}^{-1}$  for P9 complex.



**Table 6.** Calculated Values of Pauli Repulsion Energy ( $\Delta E^{\text{Pauli}}$ ), Electrostatic Energy ( $\Delta E^{\text{elec}}$ ), Orbital Interaction Energy ( $\Delta E^{\text{orb}}$ ), Dispersion Energy ( $\Delta E^{\text{disp}}$ ), and the Total Interaction Energy ( $\Delta E^{\text{total}}$ ) (in kcal mol<sup>-1</sup>) in the P9 Complex for the Dissociation into Fragments ( $\text{Eu}^{3+} + 3\text{T1} + 2\text{NO}_3^- + \text{H}_2\text{O}$ ), respectively, as obtained by using B3LYP-D3 Method with TZ2P Basis Set.

Complexes	$\Delta E^{\text{Pauli}}$	$\Delta E^{\text{elec}}$	$\Delta E^{\text{orb}}$	$\Delta E^{\text{disp}}$	$\Delta E^{\text{total}}$
P9	319.4	-1048.1 (73.5)	-330.4 (23.2)	-47.7 (3.3)	-1106.9

<sup>a</sup>Percentage contribution of  $\Delta E^{\text{elec}}$ ,  $\Delta E^{\text{orb}}$ , and  $\Delta E^{\text{disp}}$  energy to the total attractive bonding energy are provided within parenthesis.

The molecular orbitals (MOs) of the  $\text{Eu}^{3+}$  complex of T1 have been shown in the Fig.8 for P9 complex. Among these valence MOs, the low-lying MOs (SOMO, SOMO-1, SOMO-2, SOMO-3, etc.) mainly corresponds to the “p” orbitals of the O atoms of the T1,  $\text{NO}_3^-$ , and  $\text{H}_2\text{O}$  ligands for P9 complex. On the other hand, there is a significant contribution of the “f” orbitals of europium along with the “p” orbitals of the O atoms of the  $\text{NO}_3^-$  ligands in the high lying molecular orbital (LUMO) for the P9 complex as revealed from both the Fig.8.

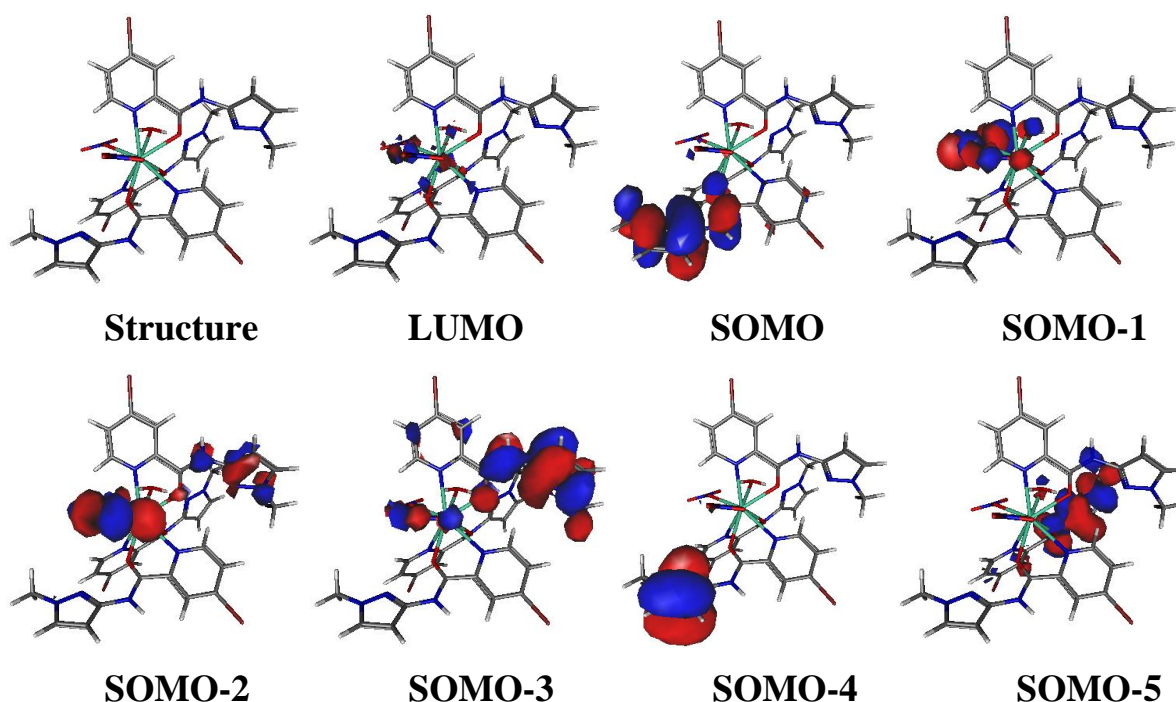


**Fig.8.** Molecular Orbital Pictures of the P9 complex,  $[\text{Eu}(\text{T1})_3(\text{NO}_3)_2(\text{H}_2\text{O})]^+$

In this context, it is interesting to discuss the prospective electrode potentials for the Eu–redox couple in P9 to compare the stability of the Eu(III) and Eu(II) form of P9. Since the most stable compound is P9 which is also found to be experimentally relevant one, therefore, the geometry of the neutral  $[\text{Eu}^{\text{II}}(\text{T1})_3(\text{NO}_3)_2(\text{H}_2\text{O})]$  complex has also been optimized using the same level of theory. We have calculated the redox potential based on the following equation

$$E_{(\text{ox})} = G_{\text{sol}}([\text{Eu}^{\text{III}}(\text{T1})_3(\text{NO}_3)_2(\text{H}_2\text{O})]^+) - G_{\text{sol}}([\text{Eu}^{\text{II}}(\text{T1})_3(\text{NO}_3)_2(\text{H}_2\text{O})]) + \text{IP1} - 4.42 \text{ versus } \text{H}^+/\text{H}_2 \text{ }^{49,50}$$

$$\dots(11)$$

where the standard hydrogen electrode (SHE) value of 4.42 V is used.<sup>51</sup> The B3LYP/def-SV(P) calculated electrode potential for  $[\text{Eu}^{\text{III}}(\text{T1})_3(\text{NO}_3)_2(\text{H}_2\text{O})]^+ / [\text{Eu}^{\text{II}}(\text{T1})_3(\text{NO}_3)_2(\text{H}_2\text{O})]$  system in P9 complex has been found to be  $-0.56 \text{ V vs SHE}$  as obtained by using the equation (11). On the other hand, the electrode potential for  $\text{Eu}^{3+}_{(\text{aq})}/\text{Eu}^{2+}_{(\text{aq})}$  is reported as  $-0.35 \text{ V vs SHE}$ .<sup>52</sup> The electrode potential of the P9 complex ( $E_{1/2} = -0.56 \text{ V vs SHE}$ ) is much more negative than that of the hydrated Eu-complex ( $E_{1/2} = -0.35 \text{ V vs SHE}$ ), which clearly indicate that the L4 ligand destabilizes the divalent state of Eu.<sup>54</sup> Therefore,  $[\text{Eu}^{\text{II}}(\text{T1})_3(\text{NO}_3)_2(\text{H}_2\text{O})]$  is lesser resistance to oxidation as compared to  $\text{Eu}^{2+}_{(\text{aq})}$ <sup>55,56</sup> which implies that the  $[\text{Eu}^{\text{III}}(\text{T1})_3(\text{NO}_3)_2(\text{H}_2\text{O})]^+$  complex is more stable than its analogous  $[\text{Eu}^{\text{II}}(\text{T1})_3(\text{NO}_3)_2(\text{H}_2\text{O})]$ .

Moreover, we have also calculated the HOMO-LUMO energy gaps ( $\Delta E_{\text{gap}}$ ) of the P9, *i.e.*,  $[\text{Eu}^{\text{III}}(\text{T1})_3(\text{NO}_3)_2(\text{H}_2\text{O})]^+$  and  $[\text{Eu}^{\text{II}}(\text{T1})_3(\text{NO}_3)_2(\text{H}_2\text{O})]$  complexes and the  $\Delta E_{\text{gap}}$  values are 2.175 and 0.938 eV, respectively, as obtained by using B3LYP method with def-SV(P) basis set. Since a higher value of  $\Delta E_{\text{gap}}$  leads to higher stability, thereby, P9 complex of  $\text{Eu}^{3+}$  is found to be more stable as compared to its  $\text{Eu}^{2+}$  counterpart.

### ***Kinetics and thermodynamics***

The  $D_{\text{Eu}}$  values were found to increase with an increase in equilibration time upto 60 min, followed by a plateau. The maximum  $D_{\text{Eu}}$  value obtained was 60. This exercise indicated that  $\sim 60 \text{ min}$  is required to achieve the equilibrium. The slower kinetics can be attributed to the high viscosity of the ionic liquid medium<sup>12</sup>. This would slow down the movement of the bulky metal-ligand complex and others, which subsequently slows down the mass transfer. A similar trend was also reported for liquid-liquid biphasic mass transfer of  $\text{Sr}^{2+}$  using substituted crown ethers in different ionic liquid analogs and extraction of  $\text{Am}^{3+}$  using different diglycolamide ligands in ionic liquids. At ambient temperature, 60 min was required to achieve equilibrium; however, at  $40^\circ\text{C}$  and  $60^\circ\text{C}$ , the time required was  $\sim 45 \text{ min}$  and  $30$

min, respectively (**Fig. 9 a**). The reduction in viscosity of the ionic liquid can be attributed to the better mass transfer kinetics, though a reduction in  $D_{Eu}$  was also noticed<sup>34</sup>.

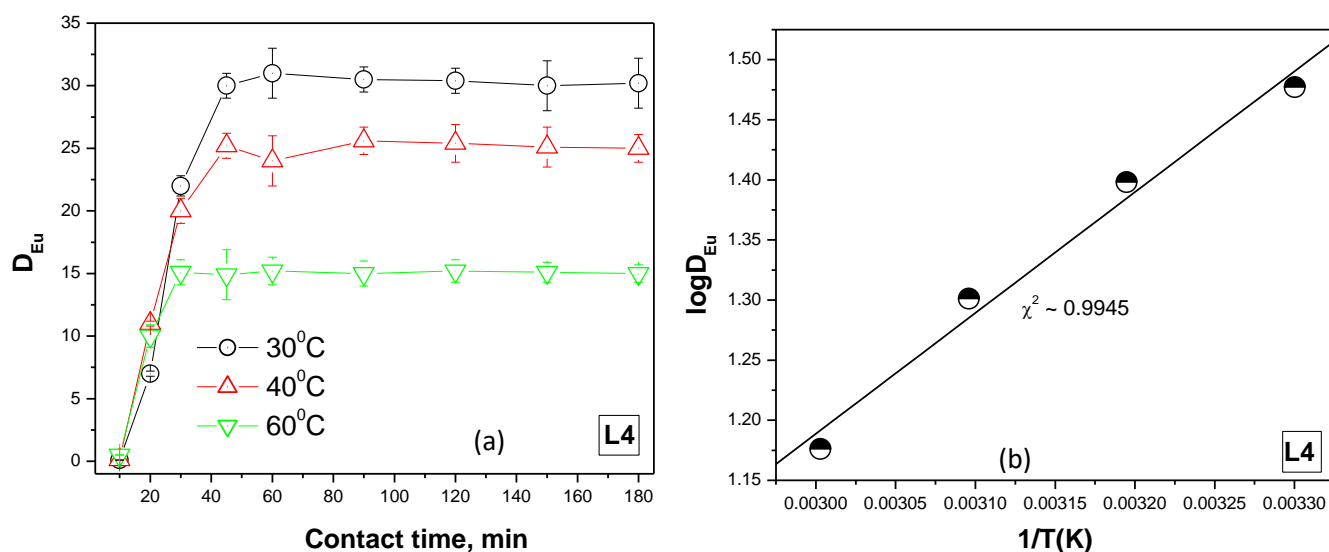


**Fig. 9** (a) Kinetics and (b) thermodynamics of liquid-liquid biphasic extractive mass transfer

The Vant Hoff equation correlates the enthalpy change of the extractive mass transfer with the equilibrium constants<sup>57</sup>, which is a direct function of  $D_{Eu}$ . **Fig. 9 (b)** depicts the variation in  $D_{Eu}$  value with temperature. At higher temperatures, the  $D_{Eu}$  value was found to decrease. It revealed the process to be exothermic. The change in enthalpy ( $\Delta H$ ) was estimated as  $-13.9 \text{ kJ mol}^{-1}$  from the slope of **Fig. 9 (b)**, whereas the change in Gibbs energy ( $\Delta G$ ) was estimated as  $-20.4 \text{ kJ mol}^{-1}$ , using the equation below. The negative  $\Delta G$  values reveal that the extractive mass transfer is spontaneous. The change in entropy is estimated as  $21.6 \text{ J K}^{-1} \text{ mol}^{-1}$ . The enhancement in overall entropy ( $\Delta S > 0$ ) can be correlated to the formation of inner sphere complex of  $\text{Eu}^{3+}$  and release of some water molecules from the primary coordination sphere of aquated  $\text{Eu}^{3+}$  ions with 9 water molecules.

$$\log K_{ex}^D = -\frac{\Delta H}{2.303 RT} + C \quad (12)$$

$$\Delta G = 2.303 RT \log K_{ex}^U \quad (13)$$

$$\Delta G = \Delta H - T\Delta S \quad (14)$$

## Conclusion

Novel amide ligand, 4-Chloro-N-(1-methyl-1H-pyrazol-3-yl)picolinamide in ionic liquid, 1-hexyl-3-methylimidazolium bis(trifluoromethylsulfonyl)imide was exploited for the extraction of  $\text{Eu}^{3+}$  ions from the aqueous acidic phase. The extractive mass transfer of  $\text{Eu}^{3+}$  ions follows a cation exchange

mechanism forming  $[\text{Eu}(\text{L})_3(\text{NO}_3)_2]^+$  type complexes. The extractive mass transfer is spontaneous and exothermic in nature. Though enhancement in entropy during mass transfer suggested the release of water molecules during complexation, the presence of one water molecule in the metal-ligand complex was evidenced by DFT calculation. Further, viscosity-induced slower extraction kinetics was observed at ambient temperature, which was improved by increasing the temperature. It is also evident that the increase in temperature decreases the extraction efficiency.

### Acknowledgement

The author acknowledges Dr. S.Kannan, Director, RC & I group, BARC and Dr. P.K.Mohapatra, Head, RCD, BARC, and Associate Director, RC & I group for their constant support and encouragement.

### Supplementary Information

The supplementary crystallographic data of  $\text{L}^4$  (CCDC number: 2205776) reported in this work can be obtained free of charge via [www.ccdc.cam.ac.uk/data\\_request/cif](http://www.ccdc.cam.ac.uk/data_request/cif), or by emailing [data\\_request@ccdc.cam.ac.uk](mailto:data_request@ccdc.cam.ac.uk), or by contacting The Cambridge Crystallographic Data Centre, 12 Union Road, Cambridge CB2 1EZ, UK; fax: +44 1223 336033.

### References:

1. (a) R. C. Ewing,; F. N. von Hippel, Nuclear waste management in the United States—Starting over, *Science* **2009**, *325* (5937), 151-152; (b) J. N. Mathur, M.S.Murali, K.L.Nash, Actinide partitioning—a review, *Solvent Extr. Ion Exch.* **2001**, *19* (3), 357-390; (c) H.H.Dam, D.N.Reinhoudt, W.Verboom, W. Influence of the platform in multicoordinate ligands for actinide partitioning, *New J. Chem.* **2007**, *31* (9), 1620-1632.
2. Y. Sasaki, Y. Sugo, K. Morita, K.L.Nash, The effect of alkyl substituents on actinide and lanthanide extraction by diglycolamide compounds, *Solvent Extr. Ion Exch.* **2015**, *33* (7), 625-641; (b) P.S. Dhama, R. Chitnis, V. Gopalakrishnan, P. Wattal, A.Ramanujam, A. Bauri, Studies on the partitioning of actinides from high level waste using a mixture of HDEHP and CMPO as extractant, *Sep. Sci. Technol.* **2001**, *36* (2), 325-335; (c) M. Weigl, A. Geist, K.Gompper, J-I Kim, Kinetics of lanthanide/actinide co-extraction with N, N'-Dimethyl-N, N'-Dibutyltetradecylmalonic Diamide (DMDBTDMA), *Solvent Extr. Ion Exch.* **2001**, *19* (2), 215-229; (d) N. Boubals, M.G.Drew, C. Hill, M.J. Hudson, P.B.Iveson, C. Madic, M.L. Russell, T.G. Youngs, *J. Chem. Soc., Dalton Trans.* **2002**, (1), 55-62; (e) S. Cao, J. Wang, C. Tan, X. Zhang, S. Li, W. Tian, H. Guo, L. Wang, Z. Qin, Solvent extraction of americium(III) and europium(III) with tridentate N,N-dialkyl-1,10-phenanthroline-2-amide-derived ligands: extraction, complexation and theoretical study, *New J. Chem.* **2016**, *40* (12), 10560-10568.
3. (a) P. R.Vasudeva Rao, Z. Kolarik, A review of third phase formation in extraction of actinides by neutral organophosphorus extractants, *Solvent Extr. Ion Exch.* **1996**, *14* (6), 955-993; (b) A. Sengupta, Sk, J. A.Boda, S. M. Ali, An amide functionalized task specific carbon nanotube for the sorption of tetra and hexa valent actinides: experimental and theoretical insight, *RSC Adv.*

- 2016**, 6 (46), 39553-39562; (c) A.Sengupta, M. S. Murali, S. K. Thulasidas, P. K. Mohapatra, Solvent system containing CMPO as the extractant in a diluent mixture containing n-dodecane and isodecanol for actinide partitioning runs, *Hydrometallurgy* **2014**, 147-148, 228-233; (d) N. Felines, G. Arrachart, F. Giusti, A. Beillard, C. Marie, S. Pellet-Rostaing, Stereochemically enriched extractants for the extraction of actinides, *New J. Chem.* **2021**, 45 (29), 12798-12801; (e) C. Li, L. Wu, L. Chen, X. Yuan, Y. Cai, W. Feng, N. Liu, Y. Ren, A. Sengupta, M.S. Murali, Highly efficient extraction of actinides with pillar[5]arene-derived diglycolamides in ionic liquids via a unique mechanism involving competitive host–guest, *Dalton Trans.* **2016**, 45 (48), 19299-19310.
4. (a) H. Eccles, Nuclear fuel cycle technologies-sustainable in the twenty first century?, *Solvent Extr. Ion Exch.* **2000**, 18 (4), 633-654; (b) J. N.Sharma, A.Kumar, V.Kumar, S.Pahan, C. Janardanan, V. Tessi, P. K.Wattal, Process development for separation of cesium from acidic nuclear waste solution using 1, 3-dioctyloxycalix [4] arene-crown-6+ isodecyl alcohol/n-dodecane solvent, *Sep. Purif. Technol.* **2014**, 135, 176-182; (c) B.A.Moyer, G. Lumetta, B.J. Mincher, In *Reprocessing and Recycling of Spent Nuclear Fuel*, Taylor, R. Ed.; Woodhead Publishing, 2015; 289-312; (d) R. Natarajan, Reprocessing of spent nuclear fuel in India: present challenges and future programme, *Prog. Nuclear Energy* **2017**, 101, 118-132.
  5. (a) Z. Yang, W. Pan, Ionic liquids: Green solvents for nonaqueous biocatalysis, *Enzyme Microb. Technol.* **2005**, 37 (1), 19-28; (b) M.J. Earle, K.R. Seddon, Ionic liquids. Green solvents for the future, *Pure Appl. Chem* **2000**, 72 (7), 1391-1398; (c) T. Welton, Ionic liquids in green chemistry, *Green Chem.* **2011**, 13 (2), 225-225; (c)R.N. Das, K. Roy, Development of classification and regression models for *Vibrio fischeri* toxicity of ionic liquids: green solvents for the future, *Toxicology Research* **2012**, 1 (3), 186-195.
  6. (a) I. Billard, A. Ouadi, C. Gaillard, Liquid–liquid extraction of actinides, lanthanides, and fission products by use of ionic liquids: from discovery to understanding, *Anal. Bioanal. Chem.* **2011**, 400 (6), 1555-1566; (b) S. Priya, A. Sengupta, Sk. Jayabun, V.C.Adya, Piperidinium based ionic liquid in combination with sulphoxides: Highly efficient solvent systems for the extraction of thorium, *Hydrometallurgy* **2016**, 164, 111-117; (c) P. Kishor, A. Sengupta, N.K. Gupta, S. Biswas, Quaternary ammonium-based task-specific ionic liquid: An efficient and 'green'separation for 'f block'elements, *Sep. Sci. Technol.* **2018**, 53 (2), 286-294; (d)A. Pandey, G. Salunkhe, V. Kathirvelu, K.S. Singh, A. Sengupta, Exploring novel functionality for efficient extraction of UO<sub>2</sub><sup>2+</sup> and Th<sup>4+</sup> in ionic liquid: Mechanism, speciation, selectivity, stability and stripping, *J. Mol. Liq.* **2021**, 324, 114716; (e) D. Das, S. Hashmi, A. Sengupta, S. Kannan, C.P. Kaushik, Understanding the extraction behaviour of UO<sub>2</sub><sup>2+</sup> and Th<sup>4+</sup> using novel picolinamide/N-oxo picolinamide in ionic liquid: A comparative evaluation with molecular diluent, *J. Mol. Liq.* **2021**, 332, 115773.
  7. (a) A. Rout, K. Venkatesan, T. Srinivasan, P.V.Rao, Extraction behavior of actinides and fission products in amide functionalized ionic liquid, *Sep. Purif. Technol.* **2012**, 97, 164-171; (b) T. Vander Hoogerstraete, B. Onghena, K. Binnemans, Homogeneous liquid–liquid extraction of metal ions with a functionalized ionic liquid, *J. Phys. Chem. Lett.* **2013**, 4 (10), 1659-1663; (c) S. Pathak, S. Biswas, A. Sengupta, Application of task specific ionic liquid for the extraction of Zirconium and Hafnium, *J. Mol. Liq.* **2021**, 338, 116616; (d) I.L. Odinet, E.V. Sharova, O.I.Artyshin, K.A.Lyssenko, Y.V. Nelyubina, G.V. Myasoedova, N.P. Molochnikova, E.A. Zakharchenro, Novel class of functionalized ionic liquids with grafted CMPO-moieties for actinides and rare-earth elements recovery, *Dalton Trans.* **2010**, 39 (17), 4170-4178; (e)F.L. Fan, Z. Qin, S.W. Cao, C.M.Tan, Q.G. Huang, D.S. Chen, J.R. Wang, X.J.

Yin, C. Xu, X.G. Feng, Highly Efficient and Selective Dissolution Separation of Fission Products by an Ionic Liquid [Hbet][Tf<sub>2</sub>N]: A New Approach to Spent Nuclear Fuel Recycling, *Inorg. Chem.* **2019**, 58 (1), 603-609.

8. (a) A.Sengupta, P.K. Mohapatra, M Iqbal, J Huskens, W Verboom, A diglycolamide-functionalized task specific ionic liquid (TSIL) for actinide extraction: solvent extraction, thermodynamics and radiolytic stability studies, *Sep. Purif. Technol.* **2013**, 118, 264-270; (b) M. Paramanik, D.R.Raut, A. Sengupta, S.Ghosh, P.K. Mohapatra, A trialkyl phosphine oxide functionalized task specific ionic liquid for actinide ion complexation: extraction and spectroscopic studies, *RSC Adv.* **2016**, 6 (24), 19763-19767; (c) P.K.Mohapatra, A. Sengupta, M. Iqbal, J. Huskens, W.Verboom, Highly efficient diglycolamide-based task-specific ionic liquids: synthesis, unusual extraction behaviour, irradiation, and fluorescence studies, *Chem. Eur. J.* **2013**, 19 (9), 3230-3238; (d) A.Sengupta, P.K. Mohapatra, P.N. Pathak, T.K. Ghanty, W Verboom, Studies on neptunium complexation with CMPO-and diglycolamide-functionalized ionic liquids: experimental and computational studies, *New J. Chem.* **2017**, 41 (2), 836-844.
9. (a) A. Rout, J. Kotlarska, W. Dehaen, K. Binnemans, Liquid–liquid extraction of neodymium (III) by dialkylphosphate ionic liquids from acidic medium: the importance of the ionic liquid cation, *Phys. Chem. Chem. Phys.* **2013**, 15 (39), 16533-16541; (b) M.L. Dietz, J.A. Dzielawa, I. Laszak, B.A.Young, M.P. Jensen, Influence of solvent structural variations on the mechanism of facilitated ion transfer into room-temperature ionic liquids, *Green Chem.* **2003**, 5 (6), 682-685; (c) X. Sun, H. Luo, S. Dai, Mechanistic investigation of solvent extraction based on anion-functionalized ionic liquids for selective separation of rare-earth ions, *Dalton Trans.* **2013**, 42 (23), 8270-8275; (d)M.L. Dietz, Ionic liquids as extraction solvents: where do we stand?, *Sep. Sci. Technol.* **2006**, 41 (10), 2047-2063.
10. A. Pandey, S. Hashmi, G. Salunkhe, V Kathirvelu, K.S. Singh, R S Chauhan, A Sengupta, Tuning the extraction mechanism of uranyl ion in bicyclooctanium, propylpyridinium, piperidinium and imidazolium based ionic liquids: First ever evidence of 'cation exchange', 'anion exchange' and 'solvation' mechanism, *J. Mol. Liq.* **2021**, 337, 116435.
11. (a) M.Singh, A.Sengupta, M.S. Murali, S.K. Thulasidas, R.M. Kadam, Selective separation of uranium from nuclear waste solution by bis(2,4,4-trimethylpentyl)phosphinic acid in ionic liquid and molecular diluents: a comparative study, *J. Radioanal. Nucl. Chem.* **2016**, 309 (3), 1199-1208; (b)M. Boltoeva, C. Gaillard, S. Georg, V.K.Karandashev, A.N. Turanov, Speciation of uranium (VI) extracted from acidic nitrate media by TODGA into molecular and ionic solvents, *Sep. Purif. Technol.* **2018**, 203, 11-19; (c) P. Nockemann, K. Servaes, R. Van Deun, K. Van Hecke, L. Van Meervelt, K. Binnemans, C. Görller-Walrand, Speciation of uranyl complexes in ionic liquids by optical spectroscopy, *Inorg. Chem.* **2007**, 46 (26), 11335-11344.
12. (a) A. Sengupta, M.S. Murali, P.K. Mohapatra, A comparative study of the complexation of Am (III) and Eu (III) with TODGA in room temperature ionic liquid, *J. Radioanal. Nucl. Chem.* **2013**, 298 (1), 405-412; (b) P.K. Mohapatra, A.Sengupta, M. Iqbal, J. Huskens, W. Verboom, Diglycolamide-Functionalized Calix[4]arenes Showing Unusual Complexation of Actinide Ions in Room Temperature Ionic Liquids: Role of Ligand Structure, Radiolytic Stability, Emission Spectroscopy, and Thermodynamic Studies, *Inorg. Chem.* **2013**, 52 (5), 2533-2541; (c) A. Sengupta, M.S. Murali, P.K.Mohapatra, M. Iqbal, J Huskens, W Verboom, An insight into the complexation of UO<sub>2</sub><sup>2+</sup> with diglycolamide-functionalized task specific ionic liquid:

- Kinetic, cyclic voltammetric, extraction and spectroscopic investigations, *Polyhedron* **2015**, *102*, 549-555; (d) A.Sengupta, P.K.Mohapatra, Extraction of radiostrontium from nuclear waste solution using crown ethers in room temperature ionic liquids, *Supramol. Chem.* **2012**, *24* (11), 771-778.
13. (a) M.Jebur, A. Sengupta, Y-H Chiao, M. Kamaz, X Qian, R.S. Wickramasinghe, Pi electron cloud mediated separation of aromatics using supported ionic liquid (SIL) membrane having antibacterial activity, *J. Membr. Sci.* **2018**, *556*, 1-11; (b) M. Kamaz, R.J.Vogler, M.Jebur, A.Sengupta, R.S. Wickramasinghe,  $\pi$  Electron induced separation of organic compounds using supported ionic liquid membranes, *Sep. Purif. Technol.* **2020**, *236*, 116237; (c) S. DePaz, A. Sengupta, Y-H Chiao, R.S. Wickramasinghe, Novel Poly (ionic liquid) Augmented Membranes for Unconventional Aqueous Phase Applications in Fractionation of Dyes and Sugar, *Polymers* **2021**, *13* (14), 2366; (d) M. Kamaz, A. Sengupta, S.S. DePaz, Y-H Chiao, R Wickramasinghe, Poly (ionic liquid) augmented membranes for  $\pi$  electron induced separation/fractionation of aromatics, *J. Membr. Sci.* **2019**, *579*, 102-110.
14. (a) N. V. Ilawe, J. Fu, S. Ramanathan, B.M. Wong, J.Wu, Chemical and radiation stability of ionic liquids: A computational screening study, *J. Phys. Chem. C* **2016**, *120* (49), 27757-27767; (b) D. Allen, G. Baston, A.E.Bradley, T.Gorman, A. Haile, I. Hamblett, J.E. Hatter, M.J. Healey, B Hodgson, R Lewin, An investigation of the radiochemical stability of ionic liquids, *Green Chem.* **2002**, *4* (2), 152-158; (c) I.A. Shkrob, T.W. Marin, S.D.Chemerisov, J.Hatcher, J.F.Wishart, Toward radiation-resistant ionic liquids. Radiation stability of sulfonyl imide anions, *J. Phys. Chem. B* **2012**, *116* (30), 9043-9055; (d) B.J. Mincher, J.F.Wishart, The radiation chemistry of ionic liquids: a review, *Solvent Extr. Ion Exch.* **2014**, *32* (6), 563-583.
15. (a) I.A.Shkrob, S.D. Chemerisov, J.F. Wishart, The initial stages of radiation damage in ionic liquids and ionic liquid-based extraction systems, *J. Phys. Chem. B* **2007**, *111* (40), 11786-11793; (b) I.A. Shkrob, T.W. Marin, J.L.Hatcher, A.R.Cook, T.Szreder, J.F. Wishart, Radiation stability of cations in ionic liquids. 2. Improved radiation resistance through charge delocalization in 1-benzylpyridinium, *J. Phys. Chem. B* **2013**, *117* (46), 14385-14399; (c) I.A. Shkrob, T. Marin, H Luo, S Dai, Radiation stability of cations in ionic liquids. 1. Alkyl and benzyl derivatives of 5-membered ring heterocycles, *J. Phys. Chem. B* **2013**, *117* (46), 14372-14384; (d) A. Sengupta, P.K.Mohapatra, A.B. Patil, R.M. Kadam, W.Verboom, Radiation stability of diglycolamide functionalized calix [4] arenes in ionic liquid: Solvent extraction, EPR and GC-MS studies, *Sep. Purif. Technol.* **2016**, *162*, 77-83.
16. (a) S. Jayabun, S. Pathak, A. Sengupta, Characterization & categorization of garnet samples for major and minor constituents by energy dispersive X-ray fluorescence spectroscopy, *Nuclear Instruments and Methods in Physics Research* **2021**, *1019*, 165854; (b) Sk. Jayabun, S Pathak, A. Sengupta, A Comprehensive Investigation alongwith the Statistical Evaluation for the Characterization of Ilmenite Mineral by X-ray Fluorescence Spectrometry and Optical Emission Spectrometry, *Chem Select* **2021**, *6* (8), 1911-1919; (c) Sk.Jayabun, A Sengupta, Development of methodologies for the chemical quality control of zircon, a precursor for zirconium production, *Chem Select* **2021**, *6* (3), 376-388.
17. G.M.Sheldrick, Crystal structure refinement with SHELXL, *Acta Crystallographica Section C: Structural Chemistry* **2015**, *71* (1), 3-8.
18. (a) A. Pandey, G.Salunkhe, V Kathirvelu, K.S.Singh, A. Sengupta, *J. Mol. Liq.* **2020**, 114716; (b) A. Pandey, S. Hashmi, V Kathirvelu, K.S. Singh, A Sengupta, Effect of alkyl chain length

- on the extraction properties of U and Th using novel CnmimNTf<sub>2</sub>/isophthalamide systems, Exploring novel functionality for efficient extraction of UO<sub>2</sub><sup>2+</sup> and Th<sup>4+</sup> in ionic liquid: Mechanism, speciation, selectivity, stability and stripping, *J. Mol. Liq.* **2021**, *323*, 114944-114948.
19. P. Devi, S.M.Barry, K.M. Houlihan, M.J. Murphy, P. Turner, M.P. Jensen, P.J. Rutledge, Synthesis and structural characterisation of amides from picolinic acid and pyridine-2, 6-dicarboxylic acid, *Sci. Rep.* **2015**, *5* (1), 9950.
  20. R. Ahlrichs, M. Bär, M. Häser, H. Horn, C. Kölmel, High-pressure supercritical carbon dioxide extraction of *Idesia polycarpa* oil: Evaluation the influence of process parameters on the extraction yield and oil quality, *Chem Phys Letters* **1989**, *162* (3), 165-169.
  21. (a) A.D. Becke, A new mixing of Hartree–Fock and local density-functional theories, *J. Chem. Phys.* **1993**, *98* (2), 1372-1377; (b) C. Lee, W. Yang, R.G. Parr, Development of the Colle-Salvetti correlation-energy formula into a functional of the electron density, *Phys. Rev. B* **1988**, *37* (2), 785-789; (c) X. Cao, M. Dolg, Segmented contraction scheme for small-core actinide pseudopotential basis sets, *M. J Mol Structure: THEOCHEM* **2004**, *673* (1-3), 203-209.
  22. A. Klamt, G. Schüürmann, COSMO: a new approach to dielectric screening in solvents with explicit expressions for the screening energy and its gradient, *J Chem Soc, Perkin Transactions 2* **1993**, (5), 799-805.
  23. (a) X. Cao, D. Heidelberg, J. Ciupka, M. Dolg, First-Principles Study of the Separation of Am<sup>III</sup>/Cm<sup>III</sup> from Eu<sup>III</sup> with Cyanex301, *Inorg. Chem.* **2010**, *49* (22), 10307-10315; (b) U. Cosentino, A. Villa, D. Pitea, G. Moro, V. Barone, Extension of computational chemistry to the study of lanthanide (III) ions in aqueous solution: Implementation and validation of a continuum solvent approach, *J. Phys. Chem. B* **2000**, *104* (33), 8001-8007.
  24. (a) R. F. W. Bader, *Atoms in Molecules - A Quantum Theory*; Oxford University Press, 1990. Biegler-könig, F. W.; Bader, R. F.; Tang, T. H. Calculation of the average properties of atoms in molecules. II. *Journal of Computational chemistry* **1982**, *3* (3), 317-328; (b) R. F. Bader, A quantum theory of molecular structure and its applications, *Chem. Rev.* **1991**, *91* (5), 893-928.
  25. T. Lu, F. Chen, Multiwfn: A multifunctional wavefunction analyzer, *J Computational Chem.* **2012**, *33* (5), 580-592.
  26. K. Morokuma, Why do molecules interact? The origin of electron donor-acceptor complexes, hydrogen bonding and proton affinity, *Acc. Chem. Res.* **1977**, *10* (8), 294-300.
  27. (a) E. Van Lenthe, A. Ehlers, E.J. Baerends, Geometry optimizations in the zero order regular approximation for relativistic effects, *J. Chem. Phys.* **1999**, *110* (18), 8943-8953; (b) G. Te Velde, F.M. Bickelhaupt, E.J. Baerends, C. Fonseca Guerra, S.J. van Gisbergen, J.G. Snijders, T. Ziegler, Chemistry with ADF, *J Comp Chem.* **2001**, *22* (9), 931-967.
  28. M. J. Montgomery, T. J. O'Connor, J. M. Tanski, Crystal structures of 4-chloro-pyridine-2-carbo-nitrile and 6-chloro-pyridine-2-carbo-nitrile exhibit different inter-molecular [π]-stacking, C-H...N nitrile and C-H...N pyridine inter-actions, *Acta Crystallographica Section E: Crystallographic Communications* **2015**, *71* (7), 852-856.



29. M. Freytag, P.G. Jones, B.Ahrens, A.K.Fischer, Hydrogen bonding and halogen–halogen interactions in 4-halopyridinium halides, *New J. Chem.* **1999**, *23* (12), 1137-1139.
30. G.E. Delgado, A.J. Mora, M. Guillén-Guillén, J.W. Ramírez, J.E. Contreras, Crystal Structure Determination and Hydrogen-Bonding Patterns in 2-Pyridinecarboxamide, *Crystal Structure Theory and Applications* **2012**, *1* (03), 30.
31. (a) P. R.Vasudeva Rao, K.A. Venkatesan, A. Rout, T.G. Srinivasan, K. Nagarajan, Potential applications of room temperature ionic liquids for fission products and actinide separation, *Sep. Sci. Technol.* **2012**, *47* (2), 204-222; (b) N. Condamines, C. Musikas, The extraction by NN-dialkylamides. II. Extraction of actinide cations, *Solvent Extr. Ion Exch.* **1992**, *10* (1), 69-100; (c) E.V. Goud, D. Das, A. Sivaramakrishna, K. Vijayakrishna, V. Sabareesh, G. Gopakumar, C.B. Rao, M.Y. Lone, P.C. Jha, Investigations on synthesis, coordination behavior and actinide recovery of unexplored dicyclohexylphosphinic acid, *Polyhedron* **2016**, *117*, 741-748.
32. (a) V.A.Cocalia, K.E. Gutowski, R.D.Rogers, The coordination chemistry of actinides in ionic liquids: A review of experiment and simulation, *Coord. Chem. Rev.* **2006**, *250* (7-8), 755-764; (b) K. Binnemans, Lanthanides and actinides in ionic liquids, *Chem. Rev.* **2007**, *107* (6), 2592-2614; (c) A.E. Visser, R.D. Rogers, Room-temperature ionic liquids: new solvents for f-element separations and associated solution chemistry, *J. Solid State Chem.* **2003**, *171* (1-2), 109-113; (d) Z. Kolarik, Ionic liquids: how far do they extend the potential of solvent extraction of f-elements?, *Solvent Extr. Ion Exch.* **2013**, *31* (1), 24-60.
33. (a) A Sengupta, R.M.Kadam, Understanding the complexation of  $\text{Eu}^{3+}$  with potential ligands used for preferential separation of lanthanides and actinides in various stages of nuclear fuel cycle: A luminescence investigation, *Spectrochimica Acta*, *173* (2017) 328–334; (b) A. Leoncini, P. K. Mohapatra, A. Bhattacharyya, D. R. Raut, Arijit Sengupta, P. K. Verma, N. Tiwari, D. Bhattacharyya, S. Jha, A.M. Wouda, J. Huskens and W. Verboom, Unique selectivity reversal in  $\text{Am}^{3+}$ – $\text{Eu}^{3+}$  extraction in a tripodal TREN-based diglycolamide in ionic liquid: extraction, luminescence, complexation and structural studies, *Dalton Trans*, 2016, *45*, 2476-2484; (c) Arijit Sengupta, Sk. Musharaf Ali, K.T.Shenoy, Understanding the complexation of the  $\text{Eu}^{3+}$  ion with TODGA, CMPO, TOPO and DMDBDMA: Extraction, luminescence and theoretical investigation, *Polyhedron*, *117*, 2016, 612–622
34. (a) A Sengupta, Lei Wu, Wen Feng, Lihua Yuan, V. Natarajan, Luminescence investigation on  $\text{Eu}^{3+}$ -pillar [5] arene-based diglycolamide (DGA) complexes: nature of the complex, Judd–Ofelt calculations and effect of ligand structure, *J Lumin*, *158*(2015)356–364.; (b) A Sengupta, Y Fang, X Yuan, L Yuan, Probing of the local environment and calculation of JO parameters for  $\text{Eu}^{3+}$  CMPO functionalized pillararene complexes by time resolved fluorescence spectroscopy, *J Lumin*, *166*,2015,187–194
35. (a) A Sengupta, P K. Mohapatra, M Iqbal, J Huskens, W Verboom, Spectroscopic investigations of  $\text{Eu}^{3+}$ -complexes with ligands containing multiple diglycolamide pendant arms in a room temperature ionic liquid, *J Lumin*, *154*,2014,392 - 401; (b) A Sengupta, S V. Godbole, P K. Mohapatra, M Iqbal, J Huskens, W Verboom, Judd–Ofelt parameters of diglycolamide-functionalized calix[4]arene  $\text{Eu}^{3+}$  complexes in room temperature ionic liquid for structural analysis: Effects of solvents and ligand stereochemistry, *J Lumin*, *148*,2014,174-180

36. (a) P K. Verma, R B. Gujar, S A. Ansari, Sk. M Ali, R J. M. Egberink, J Huskens, W Verboom, P K. Mohapatra, Sequestration of Am<sup>3+</sup> and Eu<sup>3+</sup> into ionic liquid containing Aza-macrocycle based multiple-diglycolamide ligands: Extraction, complexation, luminescence and DFT studies, *J Mol Liq.*, 2022, 347, 118291; (b) I Billard, A Ouadi, E Jobin, J Champion, C Gaillard, S Georg, Solvent Extraction and Ion Exchange 29(4):577-601; (c) A. Messadi, A. Mohamadou, S. Boudesocque, L Dupont, E. Guillon, Task-specific ionic liquid with coordinating anion for heavy metal ion extraction: Cation exchange versus ion-pair extraction, *Sep Purif Technol.*, 2013, 107, 172-178
37. J. Ciupka, X. Cao-Dolg, J. Wiebke and M. Dolg, Computational study of lanthanide (III) hydration, *Phys. Chem. Chem. Phys.*, 2010, **12**, 13215–13223.
38. J. Zhang, N. Heinz and M. Dolg, Understanding lanthanoid (III) hydration structure and kinetics by insights from energies and wave functions, *Inorg. Chem.*, 2014, **53**, 7700–7708.
39. N. Heinz, J. Zhang and M. Dolg, Actinoid (III) Hydration • First Principle Gibbs Energies of Hydration Using High Level Correlation Methods, *J. Chem. Theory Comput.*, 2014, **10**, 5593–5598.
40. L. L.-Pa´ez, E. Montes, M. Pedroni, P. H.-Gonza´lez, M. Bettinelli, D. Jaque, J. G.-Sole´ and F. Jaque, Effect of H<sub>2</sub>O and D<sub>2</sub>O Thermal Anomalies on the Luminescence of Eu<sup>3+</sup> Aqueous Complexes, *J. Phys. Chem. C*, 2018, **122**, 14838–14845.
41. M. Xia, X. Yang, Z. Chai and D. Wang, Stronger hydration of Eu (III) impedes its competition against Am (III) in binding with N-donor extractants, *Inorg. Chem.*, 2020, **59**, 6267–6278.
42. F. H. David and B. Fourest, Structure of trivalent lanthanide and actinide aquo ions, *New J. Chem.*, 1997, **21**, 167–176.
43. H. Xu, Q. Sun, Z. An, Y. Wei and X. Liu, Electroluminescence from europium (III) complexes, *Coord. Chem. Rev.*, 2015, **293–294**, 228–249.
44. K. Binnemans, Interpretation of europium (III) spectra, *Coord. Chem. Rev.*, 2015, **295**, 1–45.
45. M. Leonzio, M. Bettinelli, L. Arrico, M. Monari, L. D. Bari and F. Piccinelli, Circularly polarized luminescence from an Eu (III) complex based on 2-thenoyltrifluoroacetyl-acetonate and a tetradentate chiral ligand, *Inorg. Chem.*, 2018, **57**, 10257–10264.
46. S. T. Frey, W. DeW. Horrocks, Jr., On correlating the frequency of the 7F<sub>0</sub>→ 5D<sub>0</sub> transition in Eu<sup>3+</sup> complexes with the sum of 'nephelauxetic parameters' for all of the coordinating atoms, *Inorganica Chim. Acta*, 1995, **229**, 383–390.
47. S. A. Cotton, O. E. Noy, F. Liesener and P. R. Raithby, Unequivocal characterisation of a [Ln(terpy)(NO<sub>3</sub>)<sub>3</sub>·(H<sub>2</sub>O)] complex.: The synthesis and structure of [M(terpy)(NO<sub>3</sub>)<sub>3</sub>·(H<sub>2</sub>O)] (M=Eu, Tb); a comparison with the structure of [Eu(bipy)<sub>2</sub>(NO<sub>3</sub>)<sub>3</sub>] and with other europium nitrate complexes {terpy=2,2':6',2''-terpyridyl; bipy=2,2'-bipyridyl}, *Inorganica Chim. Acta*, 2003, **344**, 37–42.

48. D. G. Paschalidis, Synthetic and spectroscopic studies of some nitrate–lanthanide (III) hydrazone complexes of higher coordination number, *Synth. React. Inorg. Met.-Org. Chem.*, 2004, **34**, 1401–1415.
49. M. Joshi and T. K. Ghanty, Hybrid Organic–Inorganic Functionalized Dodecaboranes and Their Potential Role in Lithium and Magnesium Ion Batteries, *J. Phys. Chem. C*, 2018, **122**, 27947–27954.
50. H. Fang and P. Jena, B<sub>12</sub>(SCN)<sub>12</sub><sup>2-</sup>: An Ultrastable Weakly Coordinating Dianion, *J. Phys. Chem. C*, 2017, **121**, 7697–7702.
51. S. Trasatti, The absolute electrode potential: an explanatory note (Recommendations 1986), *Pure Appl. Chem.*, 1986, **58**, 955–966.
52. A. J. Bard and L. R. Faulkner, (2001). *Electrochemical Methods. Fundamentals and Applications* (2<sup>nd</sup> ed.). Wiley. ISBN: 9781118312803.
53. W. Zou, D. Nori-Shargh, J.E. Boggs, On the covalent character of rare gas bonding interactions: A new kind of weak interaction, *J. Phys. Chem. A* **2013**, *117* (1), 207–212.
54. S. Seibig, E. Tóth and A. E. Merbach, Unexpected Differences in the Dynamics and in the Nuclear and Electronic Relaxation Properties of the Isoelectronic [EuII(DTPA)(H<sub>2</sub>O)]<sup>3-</sup> and [GdIII(DTPA)(H<sub>2</sub>O)]<sup>2-</sup> Complexes (DTPA = Diethylenetriamine Pentaacetate)<sup>1</sup>, *J. Am. Chem. Soc.*, 2000, **122**, 5822–5830.
55. L. Burai, E. Tóth, G. Moreau, A. Sour, R. Scopelliti and A. E. Merbach, Novel Macrocyclic EuII Complexes: Fast Water Exchange Related to an Extreme M–O<sub>water</sub> Distance, *Chem.–Eur. J.*, 2003, **9**, 1394–1404.
56. (a) S. Raiguel, W. Dehaen, K. Binnemans, Extraction of gallium from simulated Bayer process liquor by Kelex 100 dissolved in ionic liquids, *Dalton Trans.* **2020**, *49* (11), 3532–3544; (b) P. Zsabka, K. Van Hecke, L. Adriaensen, A. Wilden, G. Modolo, M. Verwerft, K. Binnemans, T. Cardinaels, Selective extraction of trivalent actinides using CyMe 4 BTPPhen in the ionic liquid Aliquat-336 nitrate, *RSC Adv.* **2021**, *11* (11), 6014–6021.
57. (a) E.C.Lima, A.A. Gomes, H.N.Tran, Comparison of the nonlinear and linear forms of the van't Hoff equation for calculation of adsorption thermodynamic parameters ( $\Delta S^\circ$  and  $\Delta H^\circ$ ), *J. Mol. Liq.* **2020**, *311*, 113315; (b) M. Miguiditchian, D. Guillaumont, A. Saint-Maxent, P. Moisy, D. Guillaneux, C. Madic, Thermodynamics of plutonium (iii) and curium (iii) complexation with a N-donor ligand, *Dalton Trans.* **2019**, *48* (3), 839–842; (c) P.K. Mohapatra, A Sengupta, M. Iqbal, J Huskens, S.V. Godbole, W Verboom, Remarkable acidity independent actinide extraction with a both-side diglycolamide-functionalized calix [4] arene, *Dalton Trans.* **2013**, *42* (24), 8558–8562; (d) M.M. Maiwald, A. Skerencak-Frech, P.J. Panak, The complexation and thermodynamics of neptunium (V) with acetate in aqueous solution, *New J. Chem.* **2018**, *42* (10), 7796–7802.

## Supporting Information

### Experimental and theoretical investigation on extractive mass transfer of $\text{Eu}^{3+}$ ions using novel amide ligands in 1-hexyl-3-methylimidazolium bis(trifluoromethylsulfonyl)imide

Ayan Ghosh<sup>a,#</sup>, Amit Pandey<sup>b,#</sup>, Arijit Sengupta<sup>\*,c,d</sup>, Velavan Kathirvelu<sup>b</sup>, Sarvesh S. Harmalkar<sup>e</sup>, Sunder N. Dhuri<sup>e</sup>, Keisham S. Singh<sup>f</sup>, Tapan K. Ghanty<sup>\*,d,g</sup>,

<sup>a</sup> Laser and Plasma Technology Division, Beam Technology Development Group, Bhabha Atomic Research Centre, Trombay, Mumbai-400085, India;

<sup>b</sup>Department of Applied Sciences, National Institute of Technology Goa, Ponda, Goa 403 401, India;

<sup>c</sup>Radiochemistry Division, Bhabha Atomic Research Centre, Trombay, Mumbai-400085, India;

<sup>d</sup>HomiBhabha National Institute, Anushaktinagar, Mumbai-400094, India;

<sup>e</sup>School of Chemical Sciences, Goa University, Goa 403 206;

<sup>f</sup>Bioorganic Chemistry Laboratory, CSIR-National Institute of Oceanography, Dona Paula, Goa 403 004, India;

<sup>g</sup>Bio-Science Group, Bhabha Atomic Research Centre, Trombay, Mumbai-400085, India  
Ayan Ghosh<sup>a,#</sup>, Amit Pandey<sup>b,#</sup>, Arijit Sengupta<sup>\*,c,d</sup>, Velavan Kathirvelu<sup>b</sup>, Sarvesh S. Harmalkar<sup>e</sup>, Sunder N. Dhuri<sup>e</sup>, Keisham S. Singh<sup>f</sup>, Tapan K. Ghanty<sup>\*,d,g</sup>,

<sup>a</sup> Laser and Plasma Technology Division, Beam Technology Development Group, Bhabha Atomic Research Centre, Trombay, Mumbai-400085, India;

<sup>b</sup>Department of Applied Sciences, National Institute of Technology Goa, Ponda, Goa 403 401, India;

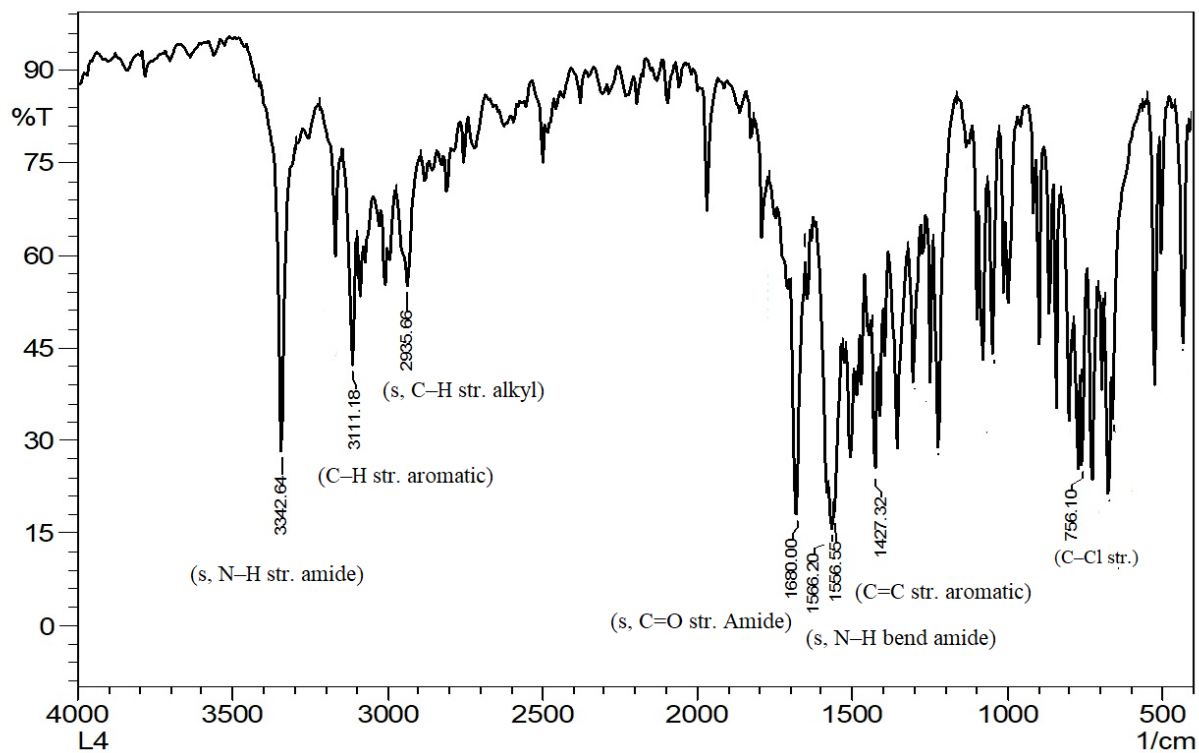
<sup>c</sup>Radiochemistry Division, Bhabha Atomic Research Centre, Trombay, Mumbai-400085, India;

<sup>d</sup>HomiBhabha National Institute, Anushaktinagar, Mumbai-400094, India;

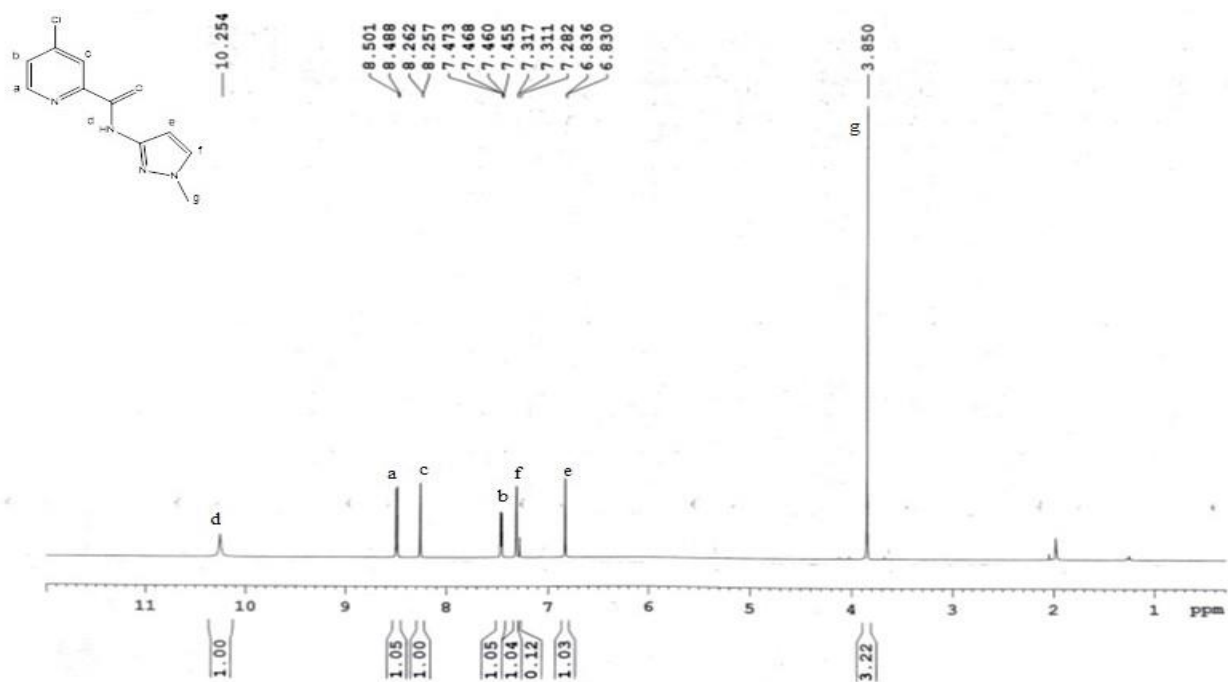
<sup>e</sup>School of Chemical Sciences, Goa University, Goa 403 206;

<sup>f</sup>Bioorganic Chemistry Laboratory, CSIR-National Institute of Oceanography, Dona Paula, Goa 403 004, India;

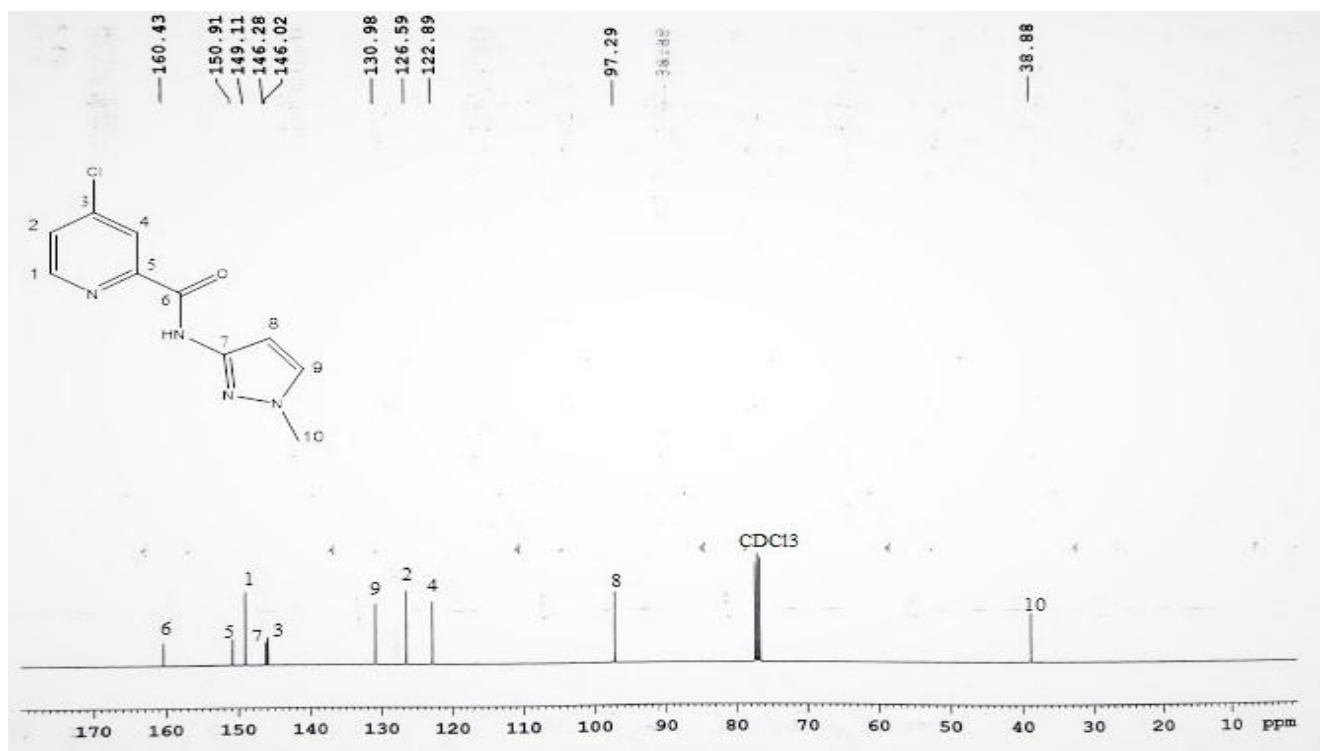
<sup>g</sup>Bio-Science Group, Bhabha Atomic Research Centre, Trombay, Mumbai-400085, India



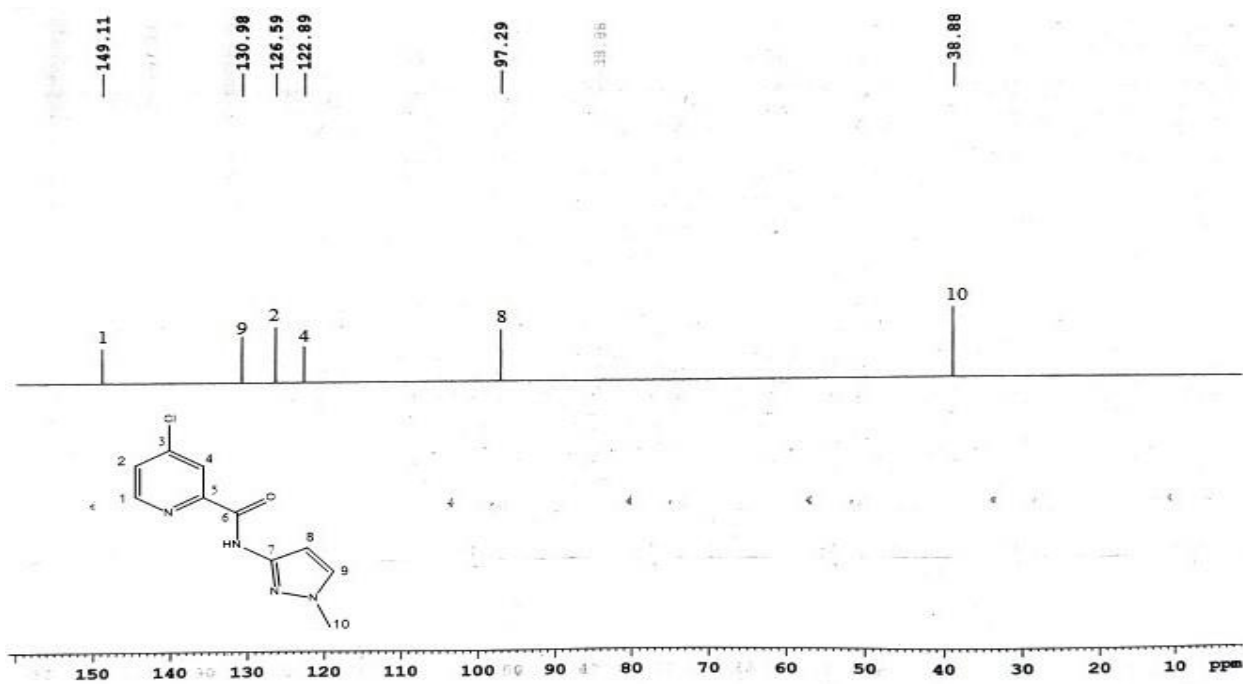
**Supplementary Fig. S1:** FT-IR Spectrum of 4-Chloro-N-(1-methyl-1H-pyrazol-3-yl)-picolinamide (L<sup>4</sup>)



**Supplementary Fig. S2:** <sup>1</sup>H NMR (400 MHz) Spectrum of 4-Chloro-N-(1-methyl-1H-pyrazol-3-yl)picolinamide (L<sup>4</sup>)

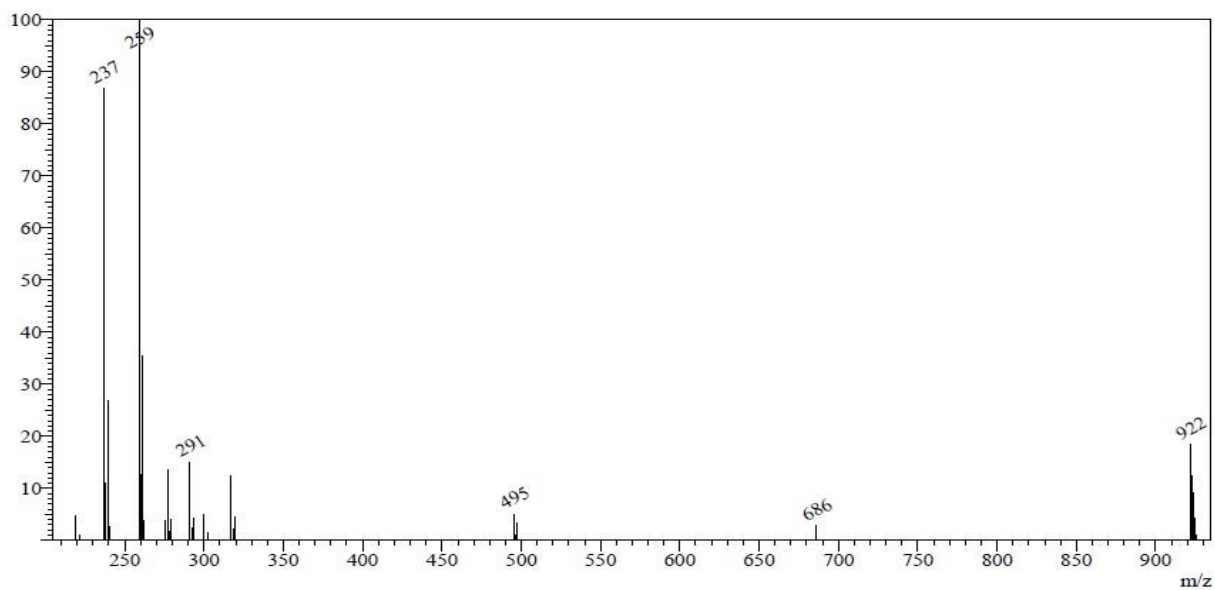


**Supplementary Fig S3:** <sup>13</sup>C NMR (100 MHz) Spectrum of 4-Chloro-N-(1-methyl-1H-pyrazol-3-yl)-picolinamide (L<sup>4</sup>)

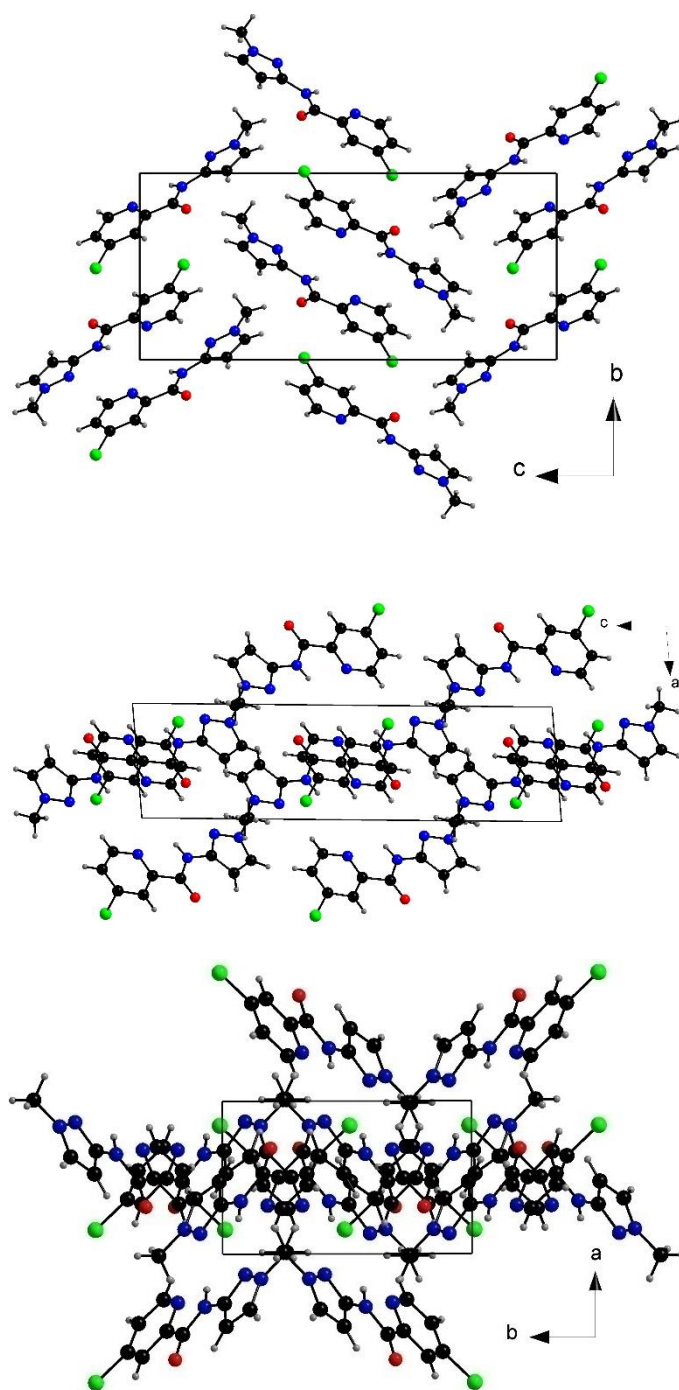


**Supplementary Fig. S4:** DEPT  $^{13}\text{C}$  NMR (100MHz) Spectrum of 4-Chloro-N-(1-methyl-1H-pyrazol-3-yl)-picolinamide ( $\text{L}^4$ )





**Supplementary Fig. S5:** LCMS Spectrum of 4-Chloro-N-(1-methyl-1H-pyrazol-3-yl)-picolinamide ( $L^4$ )



**Supplementary Fig. S6:** Crystal packing along a, b and c axis of of 4-Chloro-N-(1-methyl-1H-pyrazol-3-yl)-picolinamide ( $L^4$ )

**Supplementary Table T1:** Bond lengths (Å) in 4-Chloro-N-(1-methyl-1H-pyrazol-3-yl)picolinamide (L<sup>4</sup>)

Atom	Atom	Length(Å)	Atom	Atom	Length(Å)
C1	C2	1.372(2)	N4	C9	1.3425(19)
C1	C4	1.380(2)	N4	N3	1.3577(16)
C1	C11	1.7379(16)	N4	C10	1.4447(19)
N1	C3	1.335(2)	C4	C5	1.383(2)
N1	C5	1.3393(18)	N3	C7	1.3244(18)
O1	C6	1.2161(18)	C7	C8	1.398(2)
N2	C6	1.3462(19)	C6	C5	1.506(2)
N2	C7	1.3945(18)	C8	C9	1.367(2)
C2	C3	1.376(2)			

**Supplementary Table T2:** Bond angles (°) in 4-Chloro-N-(1-methyl-1H-pyrazol-3-yl)picolinamide (L<sup>4</sup>)

Atom	Atom	Atom	Angle (°)	Atom	Atom	Atom	Angle (°)
C2	C1	C4	120.32(15)	N3	C7	N2	117.31(12)
C2	C1	C11	120.19(12)	N3	C7	C8	112.45(13)
C4	C1	C11	119.49(13)	N2	C7	C8	130.23(13)
C3	N1	C5	116.82(14)	O1	C6	N2	124.84(14)
C6	N2	C7	126.32(12)	O1	C6	C5	121.80(14)
C1	C2	C3	118.10(15)	N2	C6	C5	113.35(12)
C9	N4	N3	111.90(12)	N1	C5	C4	124.08(14)
C9	N4	C10	128.03(13)	N1	C5	C6	116.96(13)
N3	N4	C10	120.06(12)	C4	C5	C6	118.96(13)
C1	C4	C5	117.02(14)	C9	C8	C7	104.04(13)
C7	N3	N4	103.99(11)	N4	C9	C8	107.62(13)
N1	C3	C2	123.64(15)				



The following ALERTS were generated. Each ALERT has the format  
**test-name\_ALERT\_alert-type\_alert-level.**  
Click on the hyperlinks for more details of the test.

● **Alert level C**

PLAT906_ALERT_3_C Large K Value in the Analysis of Variance .....	2.621	Check
PLAT911_ALERT_3_C Missing FCF Refl Between Thmin & STh/L= 0.600	8	Report
PLAT913_ALERT_3_C Missing # of Very Strong Reflections in FCF ....	6	Note

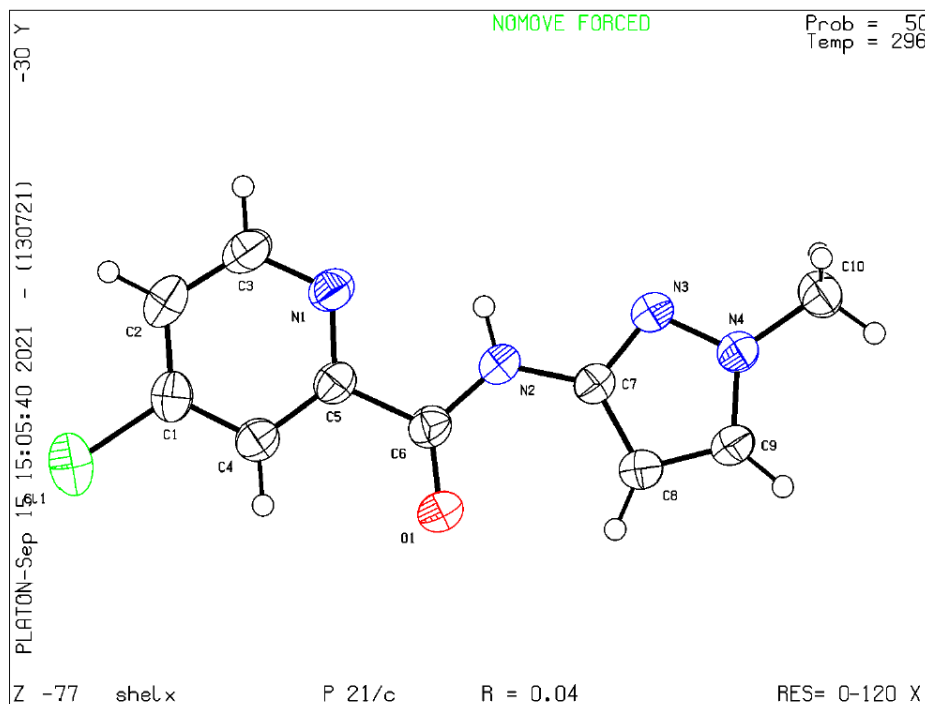
● **Alert level G**

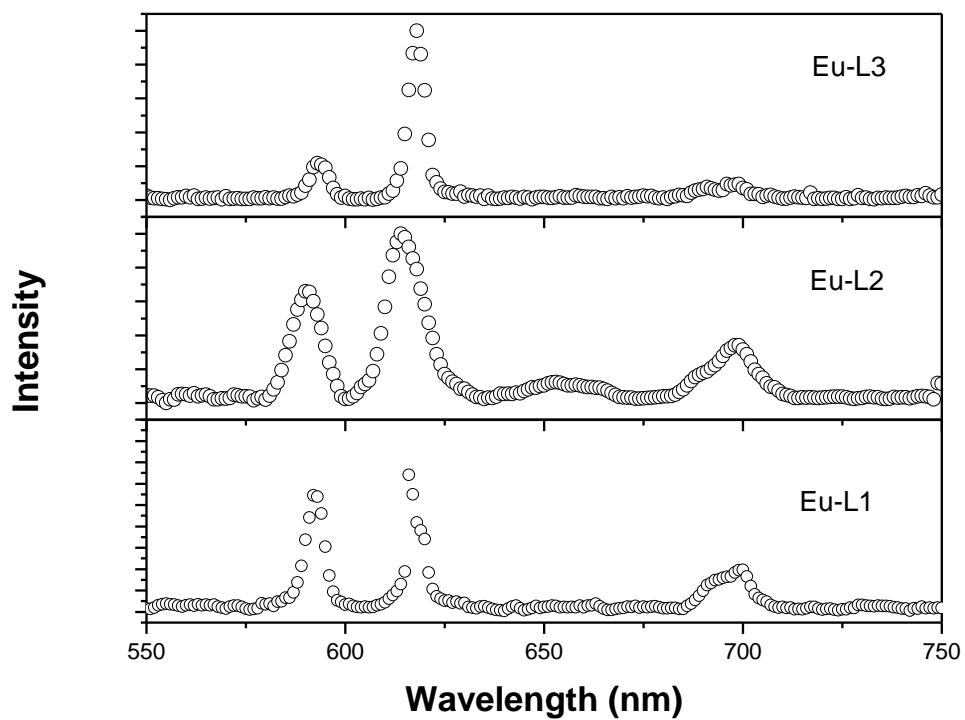
PLAT007_ALERT_5_G Number of Unrefined Donor-H Atoms .....	1	Report
PLAT883_ALERT_1_G No Info/Value for _atom_sites_solution_primary .	Please	Do !
PLAT910_ALERT_3_G Missing # of FCF Reflection(s) Below Theta(Min).	2	Note
PLAT912_ALERT_4_G Missing # of FCF Reflections Above STh/L= 0.600	6	Note
PLAT978_ALERT_2_G Number C-C Bonds with Positive Residual Density.	7	Info

- 0 **ALERT level A** = Most likely a serious problem - resolve or explain
- 0 **ALERT level B** = A potentially serious problem, consider carefully
- 3 **ALERT level C** = Check. Ensure it is not caused by an omission or oversight
- 5 **ALERT level G** = General information/check it is not something unexpected

- 1 ALERT type 1 CIF construction/syntax error, inconsistent or missing data
- 1 ALERT type 2 Indicator that the structure model may be wrong or deficient
- 4 ALERT type 3 Indicator that the structure quality may be low
- 1 ALERT type 4 Improvement, methodology, query or suggestion
- 1 ALERT type 5 Informative message, check

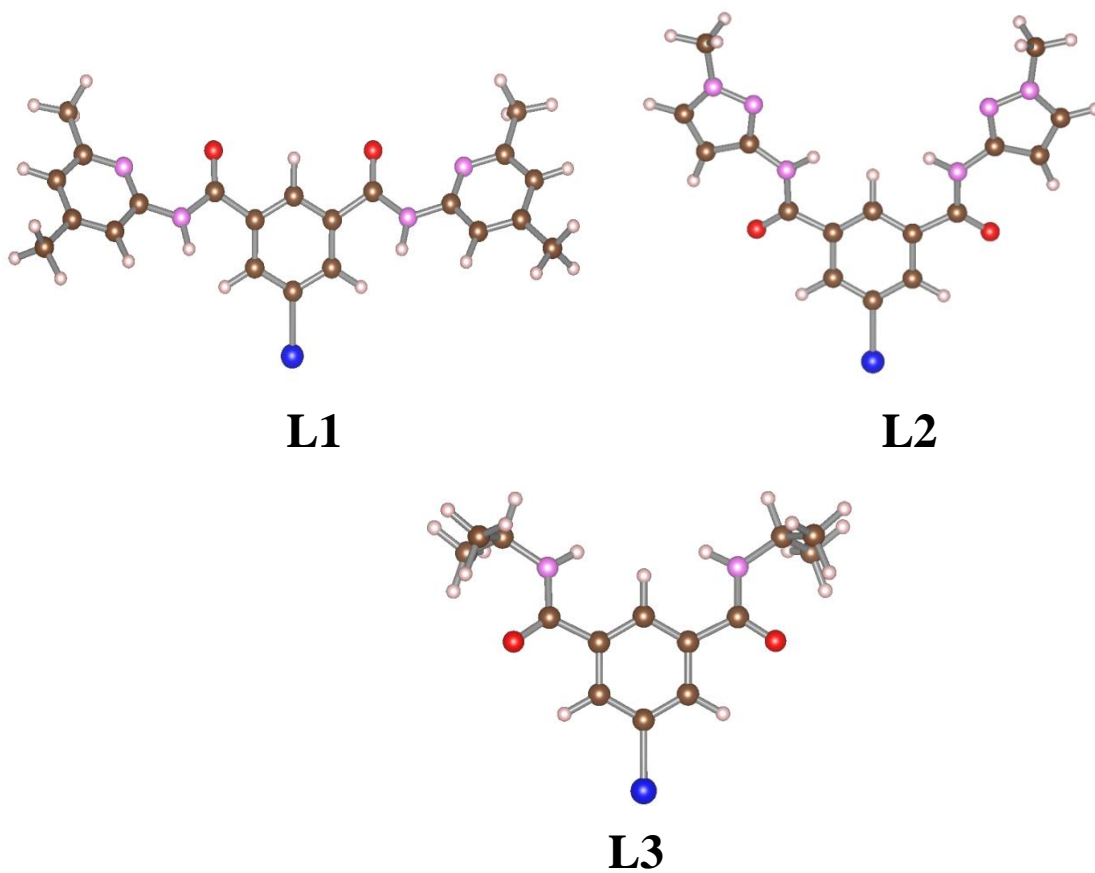
Datablock shelx - ellipsoid plot



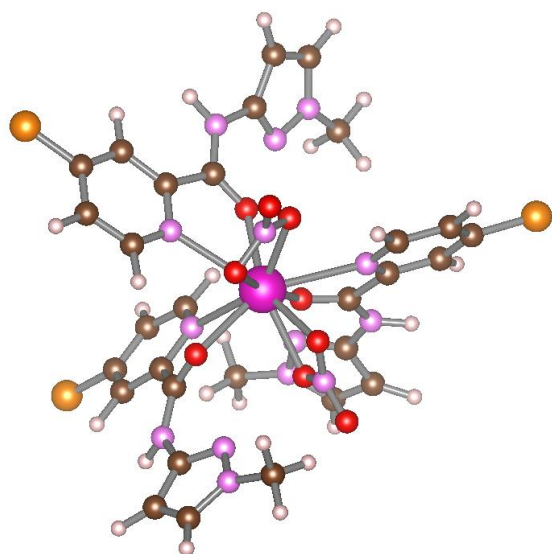


**Supplementary Fig. S 7:** Emission spectra for Eu<sup>3+</sup> complex with L1, L2 and L3 in ionic liquid

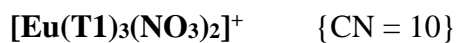
### Theoretical studies



**Supplementary Fig.S8.** Optimized structures of Ligand-1 (L1), Ligand-2 (L2), and Ligand-3 (L3) as obtained by using B3LYP method and def-SV(P) basis set. The white, dark green, pink, red, and blue represent H, C, N, O, and Br atoms, respectively.

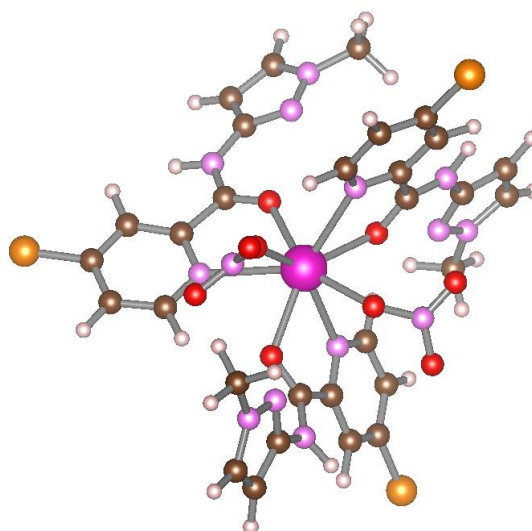


**P1**

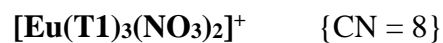


3 T1 (bidentate) + 2  $\text{NO}_3^-$  (bidentate)

*Bidentate T1 Ligand = N-donor of pyridine and O-donor of amide*

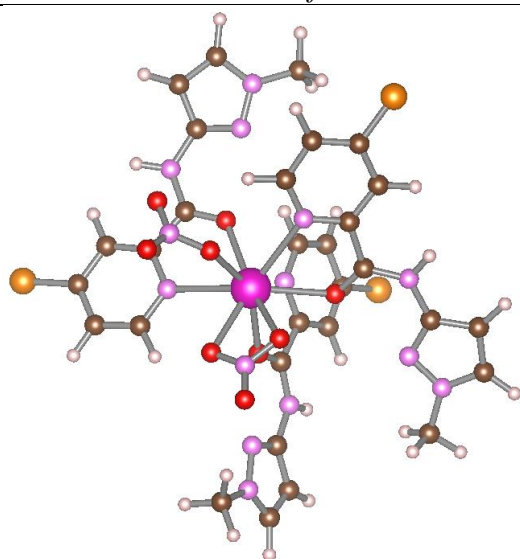


**P2**

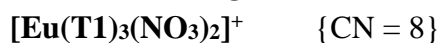


3 T1 (bidentate) + 2  $\text{NO}_3^-$  (monodentate)

*Bidentate T1 Ligand = N-donor of pyridine and O-donor of amide*



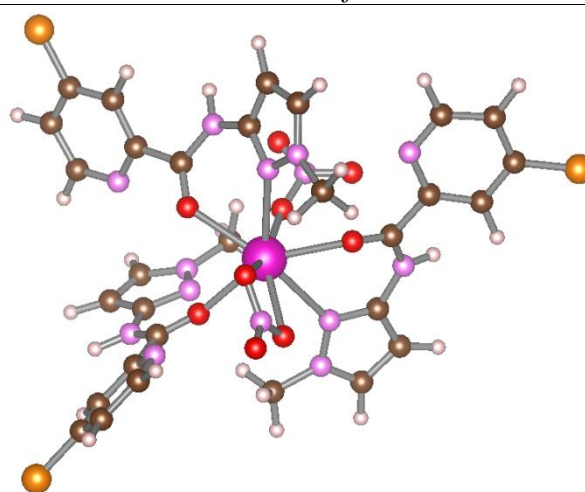
**P3**



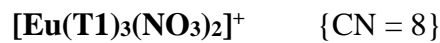
2 T1 (bidentate) + 1 T1 (monodentate) + 1  $\text{NO}_3^-$  (bidentate) + 1  $\text{NO}_3^-$  (monodentate)

*Bidentate T1 Ligand = N-donor of pyridine and O-donor of amide*

*Monodentate T1 Ligand = O-donor of amide*



**P4**

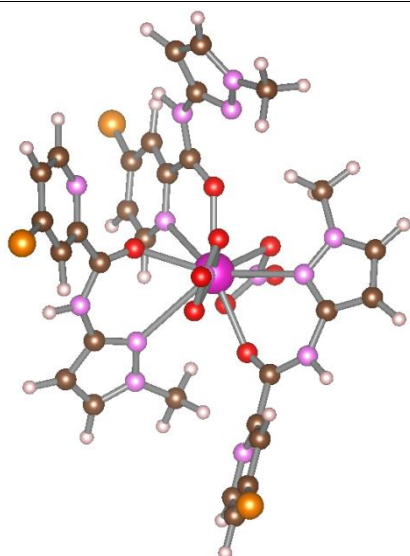


2 T1 (bidentate) + 1 T1 (monodentate) + 1  $\text{NO}_3^-$  (bidentate) + 1  $\text{NO}_3^-$  (monodentate)

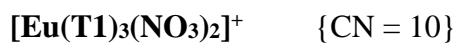
*Bidentate T1 Ligand = N-donor of pyrazole and O-donor of amide*

*Monodentate T1 Ligand = O-donor of amide*





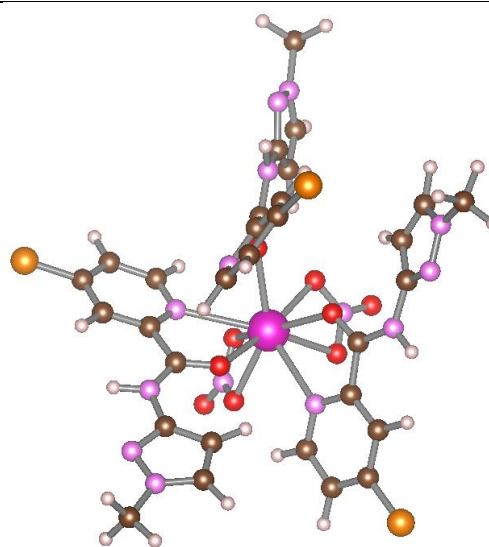
**P5**



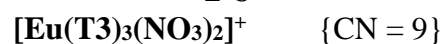
3 T1 (bidentate) + 2 NO<sub>3</sub><sup>-</sup> (bidentate)

*2 Bidentate T1 Ligand = N-donor of pyrazole and O-donor of amide*

*1 Bidentate T1 Ligand = N-donor of pyridine and O-donor of amide*



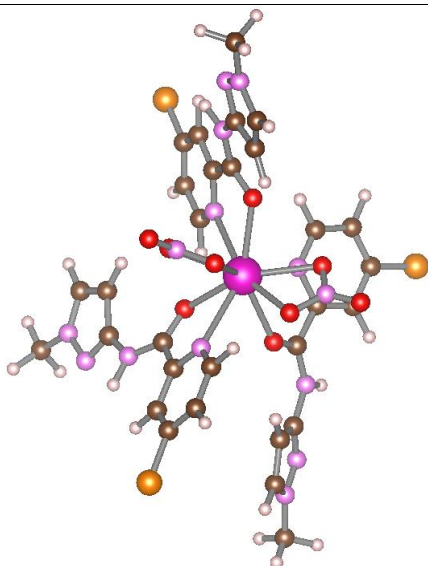
**P6**



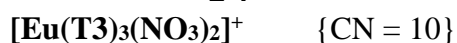
2 T3 (bidentate) + 1 T3 (monodentate) + 2 NO<sub>3</sub><sup>-</sup> (bidentate)

*Bidentate T3 Ligand = N-donor of pyridine and O-donor of amide*

*Monodentate T3 Ligand = O-donor of amide*

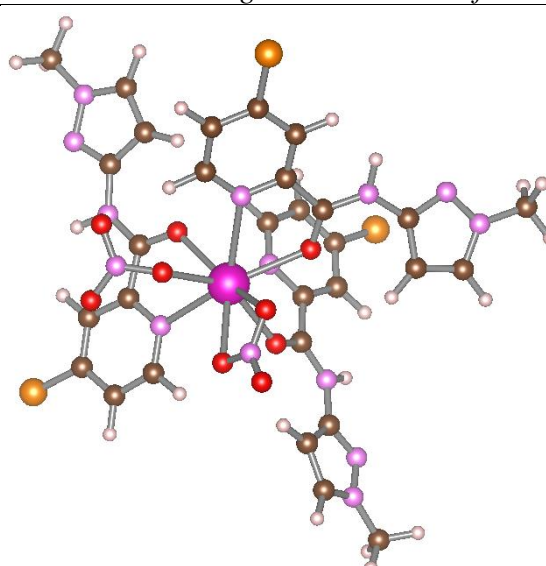


**P7**

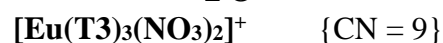


3 T3 (bidentate) + 2 NO<sub>3</sub><sup>-</sup> (bidentate)

*Bidentate T3 Ligand = N-donor of pyridine and O-donor of amide*

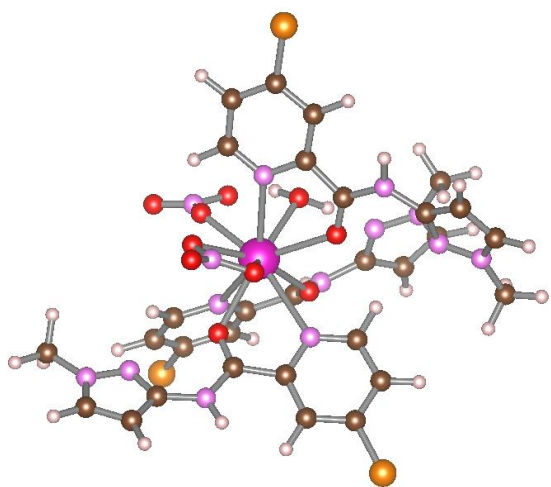


**P8**

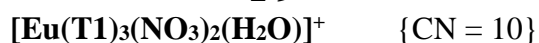


3 T3 (bidentate) + 1 NO<sub>3</sub><sup>-</sup> (bidentate) + 1 NO<sub>3</sub><sup>-</sup> (monodentate)

*Bidentate T3 Ligand = N-donor of pyridine and O-donor of amide*

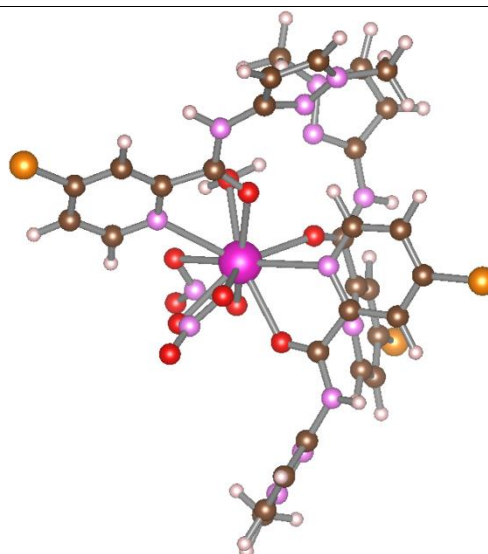


### P9

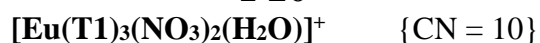


3 T1 (bidentate) + 1 NO<sub>3</sub><sup>-</sup> (bidentate) + 1 NO<sub>3</sub><sup>-</sup> (monodentate) + 1 H<sub>2</sub>O (monodentate)

*Bidentate T1 Ligand = N-donor of pyridine and O-donor of amide*



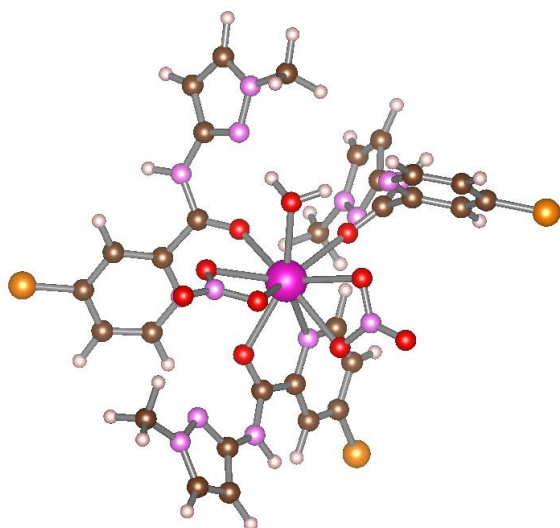
### P10



2 T1 (bidentate) + 1 T1 (monodentate) + 2 NO<sub>3</sub><sup>-</sup> (bidentate) + 1 H<sub>2</sub>O (monodentate)

*Bidentate T1 Ligand = N-donor of pyridine and O-donor of amide*

*Monodentate T1 Ligand = O-donor of amide*



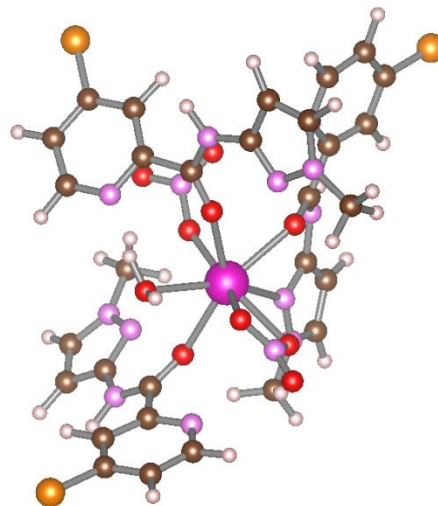
### P11



1 T1 (bidentate) + 2 T1 (monodentate) + 2 NO<sub>3</sub><sup>-</sup> (bidentate) + 1 H<sub>2</sub>O (monodentate)

*Bidentate T1 Ligand = N-donor of pyridine and O-donor of amide*

*Monodentate T1 Ligand = O-donor of amide*



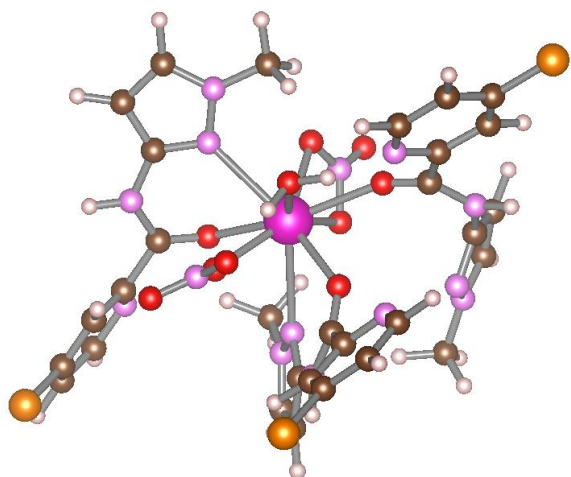
### P12



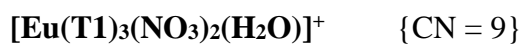
1 T1 (bidentate) + 2 T1 (monodentate) + 1 NO<sub>3</sub><sup>-</sup> (bidentate) + 1 NO<sub>3</sub><sup>-</sup> (monodentate) + 1 H<sub>2</sub>O (monodentate)

*Bidentate T1 Ligand = N-donor of pyrazole and O-donor of amide*

*Monodentate T1 Ligand = O-donor of amide*



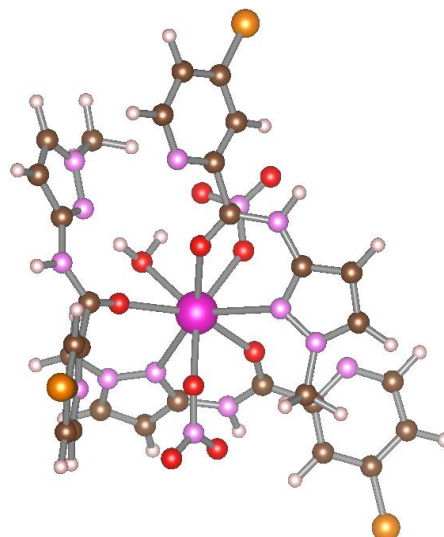
### P13



2 T1 (bidentate) + 1 T1 (monodentate) + 1  
 $\text{NO}_3^-$  (bidentate) + 1  $\text{NO}_3^-$  (monodentate) +  
 1  $\text{H}_2\text{O}$  (monodentate)

*Bidentate T1 Ligand = N-donor of pyrazole  
 and O-donor of amide*

*Monodentate T1 Ligand = O-donor of amide*



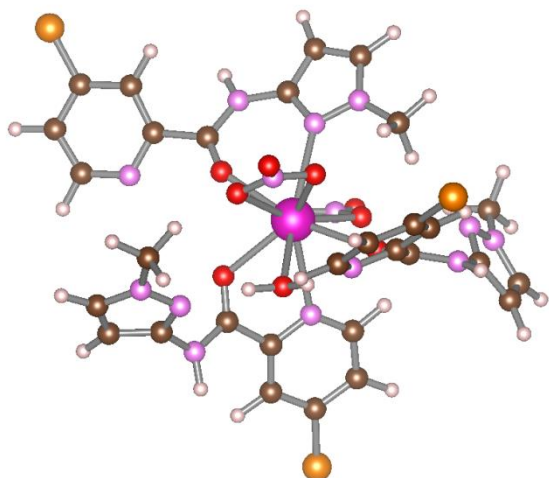
### P14



2 T1 (bidentate) + 1 T1 (monodentate) + 2  
 $\text{NO}_3^-$  (monodentate) + 1  $\text{H}_2\text{O}$  (monodentate)

*Bidentate T1 Ligand = N-donor of pyrazole  
 and O-donor of amide*

*Monodentate T1 Ligand = O-donor of amide*



### P15

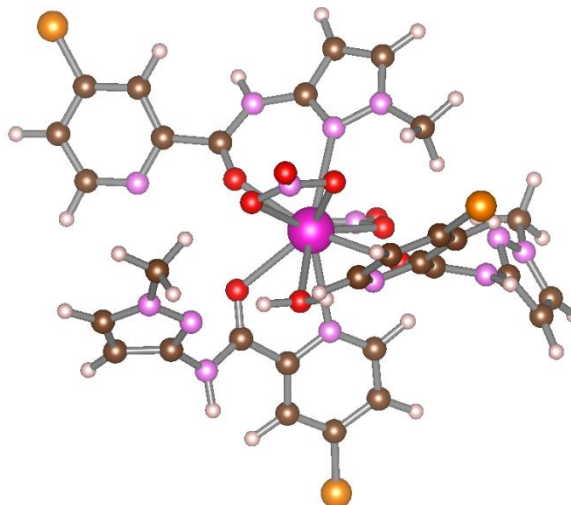


2 T1 (bidentate) + 1 T1 (monodentate) + 2  
 $\text{NO}_3^-$  (bidentate) + 1  $\text{H}_2\text{O}$  (monodentate)

*1 Bidentate T1 Ligand = N-donor of  
 pyrazole and O-donor of amide*

*1 Bidentate T1 Ligand = N-donor of pyridine  
 and O-donor of amide*

*Monodentate T1 Ligand = O-donor of amide*



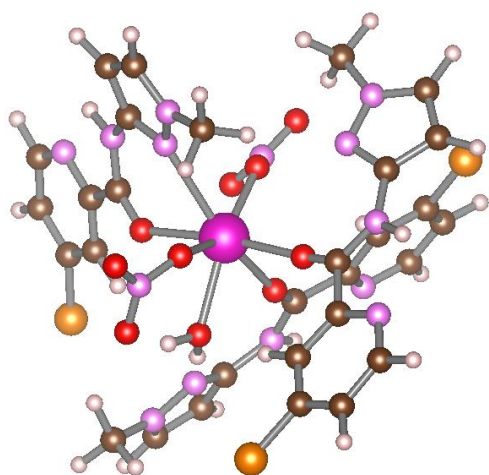
### P16



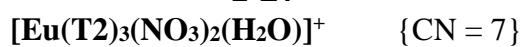
1 T2 (bidentate) + 2 T2 (monodentate) + 1  
 $\text{NO}_3^-$  (bidentate) + 1  $\text{NO}_3^-$  (monodentate) + 1  
 $\text{H}_2\text{O}$  (monodentate)

*Bidentate T2 Ligand = N-donor of pyrazole  
 and O-donor of amide*

*Monodentate T2 Ligand = O-donor of amide*



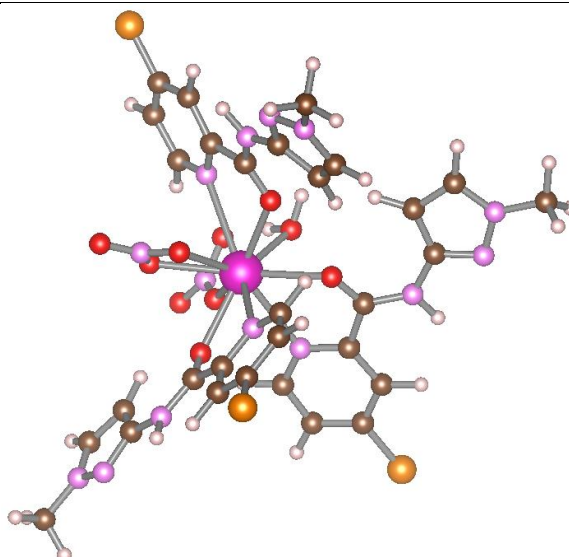
**P17**



1 T2 (bidentate) + 2 T2 (monodentate) + 2  
 $\text{NO}_3^-$  (monodentate) + 1  $\text{H}_2\text{O}$  (monodentate)

*Bidentate T2 Ligand = N-donor of pyrazole  
 and O-donor of amide*

*Monodentate T2 Ligand = O-donor of amide*

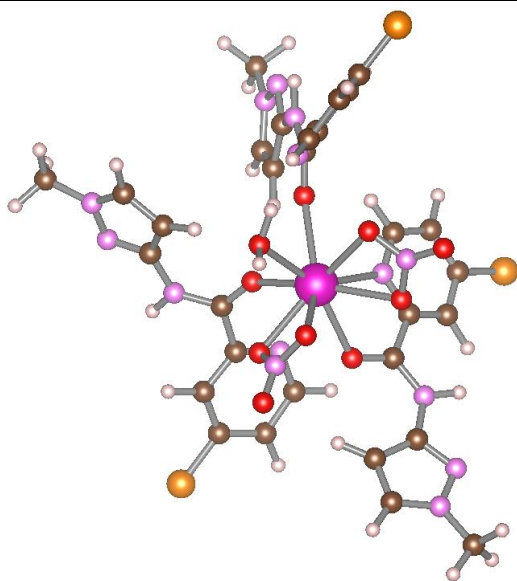


**P18**

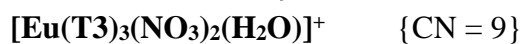


3 T3 (bidentate) + 1  $\text{NO}_3^-$  (bidentate) + 1  
 $\text{NO}_3^-$  (monodentate) + 1  $\text{H}_2\text{O}$  (monodentate)

*Bidentate T3 Ligand = N-donor of pyridine  
 and O-donor of amide*



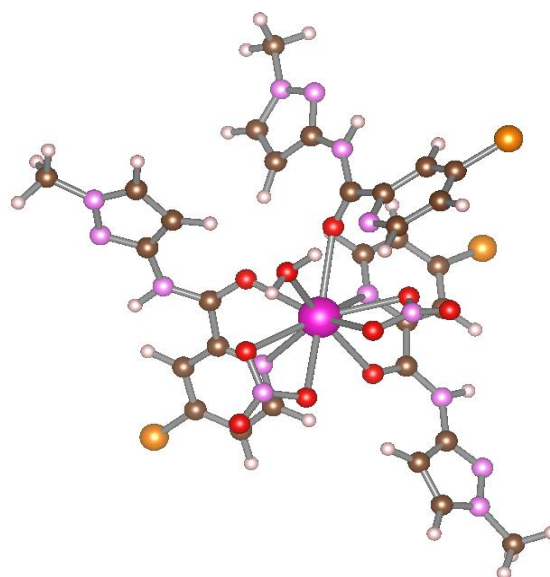
**P19**



1 T3 (bidentate) + 2 T3 (monodentate) + 2  
 $\text{NO}_3^-$  (bidentate) + 1  $\text{H}_2\text{O}$  (monodentate)

*Bidentate T3 Ligand = N-donor of pyridine  
 and O-donor of amide*

*Monodentate T3 Ligand = O-donor of amide*



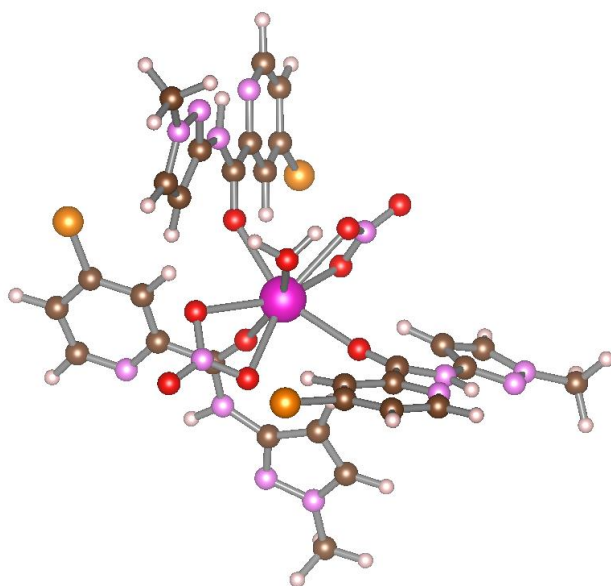
**P20**



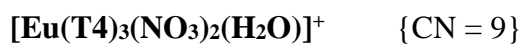
2 T3 (bidentate) + 1 T3 (monodentate) + 2  
 $\text{NO}_3^-$  (bidentate) + 1  $\text{H}_2\text{O}$  (monodentate)

*Bidentate T3 Ligand = N-donor of pyridine  
 and O-donor of amide*

*Monodentate T3 Ligand = O-donor of amide*



### P21



3 T4 (monodentate) + 2 NO<sub>3</sub><sup>-</sup> (bidentate) + 1 H<sub>2</sub>O (monodentate)

*Monodentate T4 Ligand = O-donor of amide*

**Supplementary Fig. S9.** Optimized structures of [Eu(L4)<sub>3</sub>(NO<sub>3</sub>)<sub>2</sub>]<sup>+</sup> (P1–P8) and [Eu(L4)<sub>3</sub>(NO<sub>3</sub>)<sub>2</sub>(H<sub>2</sub>O)]<sup>+</sup> (P9–P21) where L4 = T1, T2, T3, and T4, as obtained by using B3LYP method and def-SV(P) basis set. The white, dark green, pink, red, saffron, and violet represent H, C, N, O, Cl, and Eu atoms, respectively.